NASA-TM-100617 19880014454

NASA TECHNICAL MEMORANDUM 100617

STRAIN INTENSITY FACTOR APPROACH FOR PREDICTING THE STRENGTH OF CONTINUOUSLY REINFORCED METAL MATRIX COMPOSITES

C. C. POE, JR.

May 1988

NASA

National Aeronautics and Space Administration

Langley Research Center
Hampton, Virginia 23665-5225

INTRODUCTION

Metal matrix composites have relatively low densities and yet can be very strong and stiff. They can be used in more aggressive environments than resin matrix composites, and their weight saving potential is well documented. However, most fibers are elastic and their composites tend to be very notch sensitive. Ballistic impacts of unidirectional boron/aluminum caused damage that acted like a sharp notch, causing a large loss of strength [1]. Residual strengths were predicted from the fracture toughness (stress intensity factor at failure) by treating the impact damage as an equivalent crack. Thus, fracture toughness is a very important property for metal matrix composites.

The fracture toughness of composites depends on fiber and matrix properties, fiber orientations, and stacking sequence. There are far too many combinations of fiber, matrix, and layup to evaluate experimentally. Thus, some analytical guidance is needed to select fiber, matrix, and layup to give maximum fracture toughness for a given strength and stiffness. Accordingly, a maximum strain criterion was used to derive a general fracture toughness parameter that is independent of laminate orientation [2]. The fracture toughness can be predicted from the parameter using the elastic constants of the laminate and the fiber failing strain. These properties are readily obtainable. This method gave good results for resin matrix composites [3-5] but not for boron/aluminum [2].

The boron/aluminum specimens in reference [2] contained central crack-like slits and were made with various proportions of 0^0 and $\pm 45^0$ plies, including unidirectional and $[\pm 45]_{2S}$ laminates. Widespread yielding of the aluminum matrix caused the compliance to be very nonlinear, making use of the elastic constants to predict fracture toughness and strength erroneous. The degree of nonlinearity, and hence the error, increased with the proportion $\pm 45^0$ plies. Hence, in reference [2], the stress intensity factor was replaced by a strain intensity factor and the singular strain field given by the Theory of Elasticity was assumed to be valid, eliminating the elastic compliance from the equation for the general fracture toughness parameter. The strain intensity factor was derived for a uniaxially loaded specimen with a central crack. Thus, the strain intensity factor at failure, rather than the fracture toughness, was predicted. Then failing strains were predicted for the various crack lengths and strengths were calculated using stress-strain curves. The predicted strain intensity factors at failure and strengths were in good agreement with those from the experiments, even for the laminate with only $\pm 45^0$ plies. This approach should be valid for other metal matrix composites that have continuous fibers.

More recently, numerous people have calculated fiber stress concentration factors at a crack tip in metal matrix composites and accounted for yielding of the matrix. The fiber stress concentration factor is the ratio of fiber stress at the crack tip to the fiber stress away from the crack. Reedy [6,7] and Goree et al [8,9] used a discrete model for unidirectional boron/aluminum composites, and Johnson and Bigelow used an elastic-plastic finite element model [10,11] for boron/aluminum and silicon-carbide/aluminum laminates with various proportions of 0^0, $\pm 45^0$, and 90^0 plies. Reedy [7] and Goree and Jones [8] also determined how changing the aluminum yield strength affected the fiber stress concentration factor for unidirectional boron/aluminum. Post et al [12] measured the strains

at the crack tip of a $[0/\pm45]_S$ boron/aluminum specimen using moire interferometry. Goree et al [13] also calculated the fiber stress concentration factor and accounted for the effect of off-axis plies (other than 0° plies).

For both the discrete and continuum modeling [6-11,13], the specimen was assumed to fail when the stress in the fiber at the crack tip exceeded its tensile strength. It is important to note that the fiber stress failure criterion and the maximum strain criterion in reference [2] are equivalent since the stress-strain behavior of the fibers is linear. Strain equations were used in reference [2] because they are simpler than lamina (fiber) stress equations.

In this paper, the work in reference [2] is reviewed and related to other relevant and more recent work. In the first section of this paper, the material and experimental procedure of references [2,14] are described briefly for the convenience of the reader. The emphasis in this paper is on the analysis method and not the experimental data. The reader is referred to references [2,14] for more details on the material, fracture test results, and tensile stress-strain behavior. In the second section, the nonlinear stress-strain behavior of boron/aluminum is reviewed to illustrate how predictions using elastic constants result in overestimations of unnotched strength. More details are given in reference [14] for the unnotched stress-strain behavior and mechanical properties. In the third and fourth sections, the general fracture toughness parameter and the strain intensity factor for a uniaxially loaded specimen containing a central crack are reviewed. In the last section, the experimental values of the general fracture toughness parameter are presented and the predicted values of fracture toughness, strain intensity factor at failure, and strength are compared with experimental values.

NOMENCLATURE

a	half-length of crack or crack-like slit, m
b_{yy}	factor in Ramberg-Osgood equation, Pa^{-1}
E	Young's modulus, Pa
E_f	Young's modulus of fibers, Pa
F_{tu}	ultimate tensile strength of laminate (unnotched), Pa
F_{tuf}	ultimate tensile strength of fibers, Pa
K_Q	stress intenstiy factor at failure or fracture toughness, $Pa\sqrt{m}$
K_{Qe}	elastic stress intensity factor at failure, $Pa\sqrt{m}$
$K_{\epsilon Q}$	strain intensity factor at failure, $\sqrt{m}$

$K_{\epsilon Qe}$ elastic strain intensity factor at failure, $\sqrt{m}$

L length of specimen, m

n_{yy} exponent in Ramberg-Osgood equation

Q_c general fracture toughness parameter, $\sqrt{m}$

r, θ polar coordinates

S_c gross laminate (applied) stress in y-direction at failure (strength), Pa

W width of specimen, m

α fiber or ply orientation angle (relative to loading axis)

α^* angle of principal load-carrying plies

λ ratio of number of 0^0 plies to total number of plies

ϵ axial strain

ϵ_c far-field (remote or applied) strain at failure

ϵ_{tu} ultimate tensile strain of laminate (specimens without crack-like slits)

ϵ_{tuf} ultimate tensile strain of fibers

ν Poisson's ratio

ξ dimensionless material constant

$\rho_\sigma, \rho_\epsilon$ inherent crack lengths calculated from stress and strain, respectively, m

σ axial stress, Pa

Subscripts:

x,y Cartesian coordinates (The y-direction corresponds to the axial loading direction of the specimen or laminate.)

1,2 principal ply coordinates (1 refers to fiber direction)

MATERIAL AND EXPERIMENTAL PROCEDURES

The boron/aluminum composites in references [2,14] consisted of 0.142-mm-diameter (0.0056-in.) boron fibers in 6061 aluminum. The composites were tested in the as-fabricated condition. The yield strain of the aluminum was only about 0.0005, which corresponds to a strength of 34 MPa (5 ksi). The laminate orientations were $[0]_6$, $[0_2/\pm45]_S$, $[\pm45/0_2]_S$, $[0/\pm45]_S$, and $[\pm45]_{2S}$. The fiber volume fractions were 0.50 for the $[0]_6$ laminates and 0.45 for the others. The mechanical properties and stress-strain behavior are described in reference [14]. For the convenience of the reader, pertinent mechanical properties are given in Table I.

The middle cracked fracture specimens of reference [2] are shown in figure 1. The specimens were 19.1, 50.8, and 101.6 mm (0.75, 2.00, and 4.00 in.) wide and at least twice as long as wide. The crack-like slits were cut with an electrical-discharge process. The specimens were tested in a hydraulic, servo-controlled testing machine. The load was programmed to vary linearly with time at a slow rate, typically about 2 minutes to failure. Far-field strains were measured with strain gages that were located a distance from the slit of at least three times the slit length.

The unnotched tensile specimens of reference [14] were rectangular in shape and were 19.1 mm (0.75 in.) wide and 254 mm (10 in.) long. The specimens were tested in the same testing machine as the fracture specimens and with a similar load rate.

NONLINEAR STRESS-STRAIN BEHAVIOR OF BORON/ALUMINUM

Composites with fibers all in one direction do not have adequate strength and stiffness in the transverse direction for most applications. Thus, most composite laminates also contain off-axis plies, plies with fibers at some angle α to the loading direction, such as $\pm45^0$ and 90^0. When the yield strength of the matrix is exceeded, the matrix carries a lower proportion of the load than linear-elastic lamination theory predicts, particularly in the off-axis plies. The effect of yielding on the stress-strain behavior of the five boron/aluminum laminates is shown in figure 2. The specimens were loaded in the direction of the 0^0 fibers. Yielding of the aluminum causes the curves to be nonlinear. The degree of nonlinearity increases with the proportion of $\pm45^0$ plies.

For convenience, the stress-strain curves in figure 2 were calculated with the following Ramberg-Osgood equation.

$$\epsilon_y = \frac{\sigma_y}{E_y} + (b_{yy}\sigma_y)^{n_{yy}} \qquad (1)$$

The values of b_{yy} and n_{yy}, which are given in Table I, were determined in reference [14] by regression analysis of experimental data for 4 to 11 specimens

of each laminate orientation. The double subscript notation in equation (1) is taken from reference [14] to be consistent.

The effect of yielding on the tangent modulus $\frac{d\sigma_y}{d\epsilon_y}$ is shown in figure 3. The tangent modulus, which is divided by the elastic modulae E_y in Table I, was calculated from the derivative of equation (1). For small applied stresses, the Ramberg-Osgood equation does not model the tangent modulus well for laminates that contain 0° plies. The actual yield strengths are larger than indicated in figure 3. For example, the yield strength of the $[0]_6$ laminate was about 117 MPa (17 ksi), which corresponds to the aluminum yield strength of 34 MPa (5 ksi). (The laminate stress is 3.4 times the matrix stress.) The yield strength of the $[\pm 45]_{2S}$ laminates was lower, about equal to that of the aluminum. The yield strengths of laminates with both 0° and ±45° plies varied between those for $[0]_6$ and $[\pm 45]_{2S}$ according to the proportion of 0° plies. With increasing stress, the tangent modulus in figure 3 decreases and asymptotically approaches a value that corresponds to the situation where 0° fibers carry all the load. One can infer from the curves that, for small stresses in the elastic range, the aluminum matrix of the $[0]_6$ laminates carries about 20 percent of the load, and the ±45° plies of the other laminates carry from 50 to 100 percent of the load, depending on the proportion of ±45° plies. Therefore, yielding reduced the load-carrying potential of the laminates 20 to nearly 100 percent, depending on the proportion of ±45° plies.

The average failing strains for the laminates that contain 0° plies are plotted in figure 4. The failing strains were essentially equal for the different laminate orientations, 0.0076 on the average. For a fiber modulus E_f = 400 GPa (58 Msi), a strain of 0.0076 corresponds to a stress in the 0° fibers of 3.04 GPa (441 ksi), which is typical of the strength of these boron fibers. Thus, failure of these laminates coincided with failure of the 0° fibers, which carried virtually all of the load because of yielding.

For linear elastic stress-strain behavior, strengths of the laminates with 0° plies are given by

$$F_{tu} = \epsilon_{tuf} E_y \tag{2}$$

where $\epsilon_{tuf} = F_{tuf}/E_f$ is the tensile failing strain of the fibers and F_{tuf} is the tensile strength of the fibers. However, as shown in figure 5, strengths calculated with equation (2) and $\epsilon_{tuf} = 0.0076$ are much too large because of yielding, especially for laminates with ±45° plies.

On the other hand, the unnotched strengths can be predicted using the stress-strain curves rather than elastic constants. Assuming that the strains in the 0° and ±45° plies are equal at failure, the strength can be written as

$$F_{tu} = 1541\lambda + 143.8(1 - \lambda) \tag{3}$$

where λ is the proportion of 0° plies and the first and second terms give the portion of load carried by the 0° and ±45° plies, respectively. The factors 1541 and 143.8 MPa were calculated with equation (1) for the $[0]_6$ and $[\pm 45]_{2S}$ laminates, respectively, assuming $\epsilon_y = 0.0076$. Equation (3), which is plotted in figure 5 as the dashed line, is in good agreement with the data.

Strength for the $[\pm 45]_{2S}$ unnotched tensile specimens is not shown in figures 4 and 5 because the unnotched tensile specimens failed along a line that was 45° to the loading axis, indicating that failure was related to the maximum shear stress rather than the maximum tensile strength of the fibers. However, the path of the failure in specimens with cracks was mostly through the net section, indicating that failure from the crack-like slits was related to the maximum tensile strength of the fibers.

REVIEW OF GENERAL FRACTURE TOUGHNESS PARAMETER

Failure of a composite containing a crack is precipitated by failure of the principal load-carrying plies, much as in the case of unnotched laminates. The principal load-carrying plies are generally the ones with fibers most oriented with the applied load (smallest angle α in figure 6), typically 0° plies. At failure, the fiber strains ahead of a crack tip ($\theta = 0$ in figure 6) in a specially orthotropic laminate under plane stress and mode I conditions [2] can be written

$$\epsilon_{1c} = Q_c(2\pi r)^{-1/2} + B_0 + B_1 r^{1/2} + B_2 r^{3/2} + \ldots \tag{4}$$

where r is the distance from a crack tip. The coefficient Q_c is given by

$$Q_c = \frac{K_Q \xi}{E_y} \tag{5}$$

where

$$\xi = \left[1 - \frac{\nu_{yx} E_x^{1/2}}{E_y^{1/2}}\right]\left[\frac{E_y^{1/2} \sin^2 \alpha^*}{E_x^{1/2}} + \cos^2 \alpha^*\right]$$

and K_Q is the value of the stress intensity factor at failure or the fracture toughness. The angle α^* is the angle that the principal load-carrying fibers make with the y-axis in figure 6. For all the laminates containing 0° plies, $\alpha^* = 0$; and, for the $[\pm 45]_{2S}$ laminates, $\alpha^* = 45°$.

It was assumed that the principal load-carrying plies fail when the fiber strains given by equation (4) exceed a critical level. Thus, Q_c is a constant

at failure. The coefficient Q_c was referred to as a general fracture toughness parameter [2] because it is independent of laminate orientation. As noted previously, this failure criterion is equivalent to a fiber stress criterion. It follows from equation (5) that the fracture toughness K_Q is proportional to the Young's modulus E_y and the nondimensional factor ξ. The factor ξ, which is given in Table II and plotted in figure 7, is not strongly affected by the proportion of 0^o plies for the boron/aluminum laminates. Both E_y and ξ can be calculated using lamination theory. It was shown in references [3,4] for many resin matrix composites with different laminate orientations that the value of Q_c increased in proportion to the failing strain of the fibers ϵ_{tuf}. The constant of proportionality was 1.5 $\sqrt{mm}$ on the average. Thus, fracture toughness can be predicted with equation (5) from the elastic constants and the failing strain of the principal load-carrying fibers.

A STRAIN INTENSITY FACTOR

Predicting fracture toughness with equation (5) is analogous to predicting unnotched strength with equation (2). In either case, the prediction will be in considerable error if the compliance is very nonlinear. On the other hand, a strain-intensity-factor approach can be used to predict strengths of cracked specimens similar to the strain approach used to derive equation (3) for strengths of uncracked specimens. A review of the derivation in reference [2] of a strain intensity factor for uniaxially loaded specimens containing a central crack follows.

The fracture toughness or stress intensity factor at failure for a homogeneous orthotropic sheet of infinite extent, containing a central crack of length $2a$, can be written

$$K_Q = S_c\sqrt{\pi(a + \rho_\sigma) \sec (\pi a/W)} \tag{6}$$

where S_c is the applied stress at failure perpendicular to the crack and

$$\rho_\sigma = \frac{1}{\pi}\left(\frac{K_Q}{F_{tu}}\right)^2 \tag{7}$$

The constant ρ_σ was added to crack length so that $S_c = F_{tu}$, the unnotched strength, when $a = 0$. The secant function corrects for finite width. It has been verified for linear-elastic, orthotropic laminates with $2a/W < 0.5$ using finite element analyses. For example, see reference [15].

A more convenient form of equation (6) is

$$K_Q = K_{Qe}\left(1 - \frac{K_{Qe}^2}{\pi a F_{tu}^2}\right)^{-1/2} \tag{8}$$

where

$$K_{Qe} = S_c\sqrt{\pi a \sec(\pi a/W)} \tag{9}$$

For a uniaxial applied stress, the strength is

$$S_c = \epsilon_c E_y \tag{10}$$

where ϵ_c is the far-field strain at failure. Substituting equation (10) into (6),

$$K_Q = E_y K_{\epsilon Q} \tag{11}$$

where $K_{\epsilon Q}$ is the strain intensity factor at failure given by

$$K_{\epsilon Q} = \epsilon_c\sqrt{\pi(a + \rho_\epsilon)\sec(\pi a/W)} \tag{12}$$

$$\rho_\epsilon = \frac{1}{\pi}\left(\frac{K_{\epsilon Q}}{\epsilon_{tu}}\right)^2 \tag{13}$$

and ϵ_{tu} is the failing strain of the uncracked laminate. For laminates with 0^o plies, $\epsilon_{tu} = \epsilon_{tuf}$. However, in this paper, all calculations of $K_{\epsilon Q}$ were made using the values of ϵ_{tu} in Table I.

Similar to equation (6), equation (12) can be written

$$K_{\epsilon Q} = K_{\epsilon Qe}\left(1 - \frac{K_{\epsilon Qe}^2}{\pi a \epsilon_{tu}^2}\right)^{-1/2} \tag{14}$$

where

$$K_{\epsilon Qe} = \epsilon_c\sqrt{\pi a \sec(\pi a/W)} \tag{15}$$

Substituting equation (11) into (5),

$$Q_c = K_{\epsilon Q}^{\xi} \tag{16}$$

Equation (16) relates the level of strain at failure in the principal load-carrying plies ahead of a crack tip to the far-field strain. It was assumed that the level of strain at a crack tip, when normalized by the far-field strain, is not affected by widespread yielding or a nonlinear compliance, which is equivalent to assuming that the factor ξ is not affected by yielding and can be calculated with the elastic constants.

The strains ahead of a crack-like slit in a $[0/\pm45]_S$ laminate were measured by Post et al [14] using moire interferometry. Compared to the change in compliance, the level of strain in the 0^0 fiber direction normalized by the far-field strain was relatively constant with increasing applied load for points at least 0.19 mm (0.0076 in.) beyond the crack tip. This distance corresponds to the typical spacing of boron fibers, which have a diameter of 0.14 mm (0.0056 in.). However, for a point at the crack tip, the fiber strain concentration factor decreased dramatically with increasing far-field strain, from 8 to 3.

In unidirectional laminates, the discrete models [6-9,13] predict a similar reduction in fiber stress or strain concentration factor due to yielding of the aluminum in shear at the crack tips. Since the fibers have linear-elastic behavior, the fiber stress concentration factor is equal to the fiber strain concentration factor. The yield zone is less than a fiber diameter in width and extends away from a crack tip parallel to the fibers. The length of the yield zone at failure can be several times the length of the crack. However, in laminates with both 0^0 and $\pm45^0$ plies, the $\pm45^0$ plies bridge the yield zone, greatly reducing the shear stresses and the length of the yield zone [13]. Consequently, yielding in shear at the crack tip reduces the fiber strain concentration factor much more for a unidirectional laminate than for a laminate with both 0^0 and $\pm45^0$ plies, as will be evident in the experimental data.

It is important to note that the effect of yielding on fracture toughness can depend on specimen type. In reference [16], Reedy attributed differences between fracture toughness values for center-cracked, three-point-bend, and compact specimens made from unidirectional boron/aluminum to widespread yielding. Also, the fracture toughness values for three-point-bend specimens were different for different sizes, and the compact specimens split at the ends of the crack-like slit and failed without breaking fibers. In contrast, the center-cracked and three-point-bend specimens failed along a line coincident with the slit. The behavior of these specimens would probably have been less deviant had the laminates contained off-axis plies in addition to the 0^0 plies.

Also, it is interesting to note that the fiber stress concentration factor at the crack tips is reduced far more by splitting than by yielding [9,13,17]. Thus, the singular strain field given by equation (4) is not valid at all when long splits develop at the crack tips. Resin matrix composites tend to crack or split at the crack tips more so than metal matrix composites.

RESULTS AND DISCUSSION

General Fracture Toughness Parameter

Values of Q_c were calculated for each specimen using equations (14)-(16) and plotted against slit length in figures 8(a)-8(e). Average values are plotted in figure 9 for each laminate orientation and specimen width. For the $[0]_6$ specimens in figure 8(a), the values of Q_c increase with slit length. As noted previously, shear yielding at a crack tip reduces the fiber stress concentration factor and thus elevates strength and far-field failing strain. For a given applied load, the length of the yield zone and hence the reduction in the fiber stress concentration factor was shown [8,9] to increase with increasing slit length. In fact, for the long slits, the yield zones were long enough to alter measurements of remote strain [2]. The average Q_c values for $[0]_6$ in figure 9 increase with increasing specimen width because slit length increases with specimen width. For a given slit length, the values of Q_c in figure 8(a) do not appear to increase with increasing specimen width.

On the other hand, the values of Q_c for the $[0_2/\pm45]_S$, $[\pm45/0_2]_S$, and $[0_2/\pm45]_S$ laminates in figures 8(b)-8(c) do not increase noticeably with slit length. As noted previously, the fiber stress concentration factor is reduced less by shear yielding at the crack tips when laminates contain both 0° and $\pm45^\circ$ plies than when laminates contain only 0° plies. However, the average values of Q_c in figure 9 for these laminates do increase with increasing specimen width, and the increase is greater with increasing proportion of $\pm45^\circ$ plies.

For $[\pm45]_{2S}$ specimens with short slits, the far-field strains at failure reported in reference [2] were very large, much as those for the unnotched specimens. For wide specimens, the resulting values of Q_c were so large that a larger scale had to be used for figure 8(e) than for figures 8(a)-8(d). On the other hand, far-field strains at failure for the wide $[\pm45]_{2S}$ specimens with long slits were less than one-tenth those with short slits, causing the Q_c values in figure 8(e) to decrease with increasing slit length. In fact, for wide specimens with the longest slits, far-field strains at failure for $[\pm45]_{2S}$ specimens were as small as those for specimens containing 0° plies. For this reason, the average values of Q_c in figure 9 vary greatly with specimen width.

For $[\pm45]_{2S}$ specimens with long slits, the values of Q_c in figure 8(e) are considerably larger for the 101.6-mm-wide (4.00-in.) specimens than for the 50.8-mm-wide (2.00-in.) specimens. Notice how the unnotched strengths in Table I increase with specimen width. Therefore, the increase of Q_c values with specimen width for $[0_2/\pm45]_S$, $[\pm45/0_2]_S$, $[0_2/\pm45]_S$, and $[\pm45]_{2S}$ laminates is probably related to the $\pm45^\circ$ plies.

It was previously noted that the unnotched $[\pm 45]_{2S}$ specimens failed on a plane oriented at 45° to the applied load, indicating that the failure was associated with the maximum shear stress. On the other hand, the $[\pm 45]_{2S}$ specimens with slits failed along a line that was more or less coincident with the slit, which is consistent with tensile failure of the fibers.

As shown in figure 9, an average value of Q_c for laminates containing 0° plies and for specimens wider than 19.1 mm (0.75 in.) is 0.0121 $\sqrt{mm}$. It was shown [3,4] for many composite materials and laminate orientations that the value of Q_c increased in proportion to the failing strain of the fibers ϵ_{tuf}. The constant of proportionality was 1.5 $\sqrt{mm}$ on the average. Taking ϵ_{tuf} = 0.00760, and Q_c = 0.0121 $\sqrt{mm}$ for the boron/aluminum, Q_c/ϵ_{tuf} = 1.59 $\sqrt{mm}$, which is reasonably close to 1.5 $\sqrt{mm}$.

Strain and Stress Intensity Factors at Failure

The values of $K_{\epsilon Q}$ calculated with equations (14) and (15) were averaged for each specimen width and plotted against the percent of 0° plies in figure 10, as well as recorded in Table II. Values predicted using equation (16) with the ξ values in Table II and Q_c = 0.0121 $\sqrt{mm}$ are plotted as a line for comparison. Equation (16) is in good agreement with the test data except for the $[\pm 45]_{2S}$ laminates. Again, for the $[\pm 45]_{2S}$ laminates, the very large far-field strains at failure for wide specimens with short slits elevated the Q_c values. Notice that the predicted value of $K_{\epsilon Q}$ is relatively constant with increasing proportion of 0° plies, indicating that the far-field strains at failure for the various laminate orientations are also nearly equal for a given slit length [2].

Average values of fracture toughness or stress intensity factor at failure calculated with equations (8) and (9) are plotted similarly in figure 11, as well as recorded in Table II. The solid line was predicted using equation (5), the elastic constants and ξ values in Table II, and Q_c = 0.0121 $\sqrt{mm}$. Except for the $[0]_6$ laminates, the solid line is far above the test data, much as in figure 5 for the unnotched tensile strength. In effect, widespread yielding caused the laminates with and without slits to be weaker than linear-elastic theory predicted. The dashed line was also calculated with equation (5) except that E_y was replaced by the secant modulus F_{tu}/ϵ_{tu}. The test data and the dashed curve are in fairly good agreement.

For silicon-carbide/aluminum laminates, Johnson and Bigelow [11] predicted trends similar to those in figure 11 using an elastic-plastic finite element model. For laminates with both 0° and off-axis plies, they found that the fiber stress at the crack tip for a given applied laminate stress or load was more when yielding occured than when the material was elastic, indicating that widespread yielding causes a cracked laminate to be weaker than predicted by linear-elastic theory. However, for a unidirectional laminate, they found that

the fiber stress at the crack tip was less when yielding occured than when the material was elastic, indicating that shear yielding at the crack tips causes a cracked laminate to be stronger than predicted by linear-elastic theory. Therefore, the analysis in reference [11] and the results of this paper show that shear yielding at the crack tip increases the strength of a unidirectional laminate, whereas widespread yielding decreases the strength of a laminate with 0^0 and off-axis plies.

Strength Predictions

Values of $K_{\epsilon Q}$ were predicted for each laminate orientation using equation (16) with $Q_c = 0.0121$ $\sqrt{mm}$ and the ξ values in Table II. Then, far-field strains at failure were calculated using equations (14) and (15) with $Q_c = 0.0121$ $\sqrt{mm}$ and the ϵ_{tu} values in Table I, and strengths were calculated using equation (1), the Ramberg-Osgood equation. This approach is analogous to using equation (3) to predict unnotched strength. Strengths were also predicted directly with the stress intensity factor using equations (5), (8), and (9) with $Q_c = 0.0121$ $\sqrt{mm}$, $E_y = F_{tu}/\epsilon_{tu}$, and the values of F_{tu} and ϵ_{tu} in Table I. Both predictions of strength are plotted in figures 12(a)-12(e) along with the experimental strengths for all five laminate orientations. The strengths were multiplied by the secant correction factor to make the strengths for the different specimen widths coalesce. For this reason, only one curve is shown for the direct predictions of strength using the stress intensity factor except for the $[\pm 45]_{2S}$ specimens in figure 12(e). Here, a different unnotched strength was used for each specimen width. On the other hand, the strength curves predicted from the strains do not exactly coalesce. However, except for the $[\pm 45]_{2S}$ specimens, the curves do not differ significantly for $2a < W/2$. Strengths were not predicted for $2a > W/2$ since the accuracy of the secant correction factor is questionable. The strengths predicted from the strains and the experimental strengths are in fairly good agreement, even for the $[\pm 45]_{2S}$ specimens. The strengths predicted directly with the stress intensity factor and the experimental strengths are also in fairly good agreement, except for the $[\pm 45]_{2S}$ specimens. The deviation between the strengths predicted from the strains and the stress intensity factor increases with the proportion of $\pm 45^0$ plies.

CONCLUSIONS

The method developed in reference [2] to predict fracture toughness of boron/aluminum laminates does not work because widespread yielding of the aluminum causes the compliances to be very nonlinear. An alternate method was developed to predict a strain intensity factor at failure. Singular strain fields from the Theory of Elasticity were assumed to be valid despite the widespread yielding. These strains are proportional to a strain intensity factor, just as the singular stress field is proportional to the stress intensity factor. A general fracture toughness parameter Q_c, which is

independent of laminate orientation, is proportional to the strain intensity factor at failure and another factor that depends on the elastic constants of a laminate. Values of strain intensity factors at failure were predicted for specimens containing central crack-like slits. The specimens were made from five different laminate orientations: $[0]_6$, $[0_2/\pm45]_S$, $[\pm45/0_2]_S$, $[0/\pm45]_S$, and $[45]_{2S}$. The nonlinearity of the stress-strain curves increased with the proportion of $\pm45^0$ plies. Failing strains were predicted from the strain intensity factors at failure, and strengths were predicted from the failing strains using uniaxial stress-strain curves.

The predicted and measured strain intensity factors at failure and strengths were in generally good agreement. On the other hand, the fracture toughness values for laminates with 0^0 and off-axis plies were overestimated using the elastic constants. However, it was shown that, except for the $[\pm45]_{2S}$ specimens, the fracture toughness could be predicted fairly accurately using the secant modulus in place of the elastic Young's modulus. This method should be valid for other metal matrix composites with continuous fibers. Johnson and Bigelow [11] using an elastic-plastic finite element model also found that elastic theory overestimates strength for laminates with 0^0 and off-axis plies.

Although the tests and predictions were in generally good agreement, several discrepancies were observed: (1) The values of Q_c for the $[0]_6$ specimens increased with slit length because the fiber stress at the ends of a slit were reduced by yielding in shear. Likewise, the experimental strengths were 10-20 percent greater than the predicted strengths for long slits. For laminates with both 0^0 and $\pm45^0$ plies, the yielding in shear was not significant, and the values of Q_c were independent of slit length. (2) The values of Q_c for the $[45]_{2S}$ specimens decreased with slit length. The far-field failing strains for specimens with short slits were nearly ten times those for specimens with long slits. The linear-elastic analysis did not completely account for this difference. (3) For laminates that contained $\pm45^0$ plies, the values of Q_c increased with increasing specimen width. Strengths increased similarly. This effect increased with increasing proportion of $\pm45^0$ plies.

REFERENCES

1. Jaques, Capt., USAF; W. J.: Soft Body Impact Damage Effects on Boron-Aluminum Composites. AFML-TR-74-155, Air Force Materials Laboratory, Jan. 1975.

2. Poe, Jr., C. C.: Fracture Toughness of Boron/Aluminum Laminates with Various Proportions of 0^0 and $\pm45^0$ Plies. NASA TP-1707, 1980.

3. Poe, Jr., C. C.: A Unifying Strain Criterion for Fracture of Fibrous Composite Laminates. Engineering Fracture Mechanics, vol. 17, no. 2, 1983, pp. 153-171.

4. Poe, Jr., C. C.: Fracture Toughness of Fibrous Composite Materials. NASA TP-2370, November 1984.

5. Poe, Jr., C. C.: A Parametric Study of Fracture Toughness of Fibrous Composite Materials. NASA TM-89100, February 1987.

6. Reedy, Jr., E. D.: Analysis of Center-Notched Monolayers with Application to Boron/Aluminum Composites. Journal of Mechanics and Physics of Solids, Vol. 28, 1980, pp 265-286.

7. Reedy, Jr., E. D.: Notched Unidirectional Boron/Aluminum: Effect of Matrix Properties. Journal of Composite Materials, Vol. 16, (1982), pp.495-509.

8. Goree: J. G.; and Jones, W. F.: Fracture Behavior of Unidirectional Boron/Aluminum Composite Laminates. NASA CR-3753, December, 1983.

9. Goree: J. G.; and Gross, R. S.: Analysis of a Unidirectional Composite Containing Broken Fibers and Matrix Damage. Engineering Fracture Mechanics, Vol. 13, 1979, pp. 563-578.

10. Johnson, W. S.; Bigelow, C. A.; and Bahei-El-Din, Y. A.: Experimental and Analytical Investigation of the Fracture Processes of Boron/Aluminum Laminates Containing Notches. NASA TP-2187, September 1983.

11. Johnson, W. S.; and Bigelow, C. A.: Elastic-Plastic Stress Concentrations around Crack-Like Notches in Continuous Fiber Reinforced Metal Matrix Composites. NASA TM-89093, February 1987.

12. Post, D.; Czarnek, R.; Joh, D.; Jo, J.; and Guo, Y: Elastic-Plastic Deformation of a Metal-Matrix Composite Coupon with a Center Slot. NASA CR-178013, November 1985.

13. Goree: J. G.; and Kaw, A. K.: Shear-Lag Analysis of Notched Laminates with Interlaminar Debonding. NASA CR-3798, May, 1984.

14. Sova, J. A.; and Poe, Jr., C. C.: Tensile Stress-Strain Behavior of Boron/Aluminum Laminates. NASA TP-1117, 1978.

15. Tan, P. W.; and Bigelow, C. A.: Analysis of Cracked Laminates with Holes Using the Boundary Force Method. Proceedings of the AIAA/ASEM/ASCE/AHS 28th Structures, Structural Dynamics and Materials Conference, Monterey, A, April 6-8, 1987, paper no. AIAA-87-0862-CP.

16. Reedy, Jr. E. D.: On the Specimen Dependence of Unidirectional Boron/Aluminum Fracture Toughness. Journal of Composite Materials Supplement, Vol. 14, (1980), pp.118-131.

17. Goree: J. G.; and Wolla, M. W.: Longitudinal Splitting in Unidirectional Composites, Analysis and Experiments. NASA CR-3881, April, 1985.

Table I. Tensile properties of unnotched laminates.

Laminate orientation	F_{tu}, MPa	ϵ_{tu}	ν_{yx}	E_x, MPa	E_y, MPa	b_{yy}, NPa^{-1}	n_{yy}
W = 19.1 mm							
$[0]_6$	1672.0	0.007908	0.2049	143.1	237.3	7.178	1.511
$[0_2/\pm45]_S$	800.1	.007267	.2513	130.1	176.2	27.97	1.539
$[\pm45/0_2]_S$	910.5	.008205	.2519	134.7	177.5	24.07	1.504
$[0/\pm45]_S$	581.4	.007008	.2911	129.5	159.2	68.10	1.743
$[\pm45]_{2S}$	220.6	[a].04974	.3247	126.2	126.9	2371.	4.682
W = 50.8 mm							
$[\pm45]_{2S}$	280.8	[a].1511	-	-	-	-	-
W = 101.6 mm							
$[\pm45]_{2S}$	330.9	[a].3237	-	-	-	-	-

[a] - Calculated with Ramberg-Osgood equation for W = 19.1 mm.

Table II. Stress and strain intensity factors at failure.

Laminate orientation	ξ	K_Q, MPa$\sqrt{mm}$, for W -			$K_{\epsilon Q}$, $\sqrt{mm}$, for W -		
		19.1 mm	50.8 mm	101.6 mm	19.1 mm	50.8 mm	101.6 mm
$[0]_6$	0.8409	2184	3495	3854	0.01091	0.01602	0.01794
$[0_2/\pm45]_S$	.7841	1400	1719	1832	.01251	.01331	.01443
$[\pm45/0_2]_S$	.7806	-	1699	1821	-	.01348	.01416
$[0/\pm45]_S$	.7375	1239	1615	1808	.01454	.01614	.01856
$[\pm45]_{2S}$	.6771	345	707	703	.02185	.03845	.02782

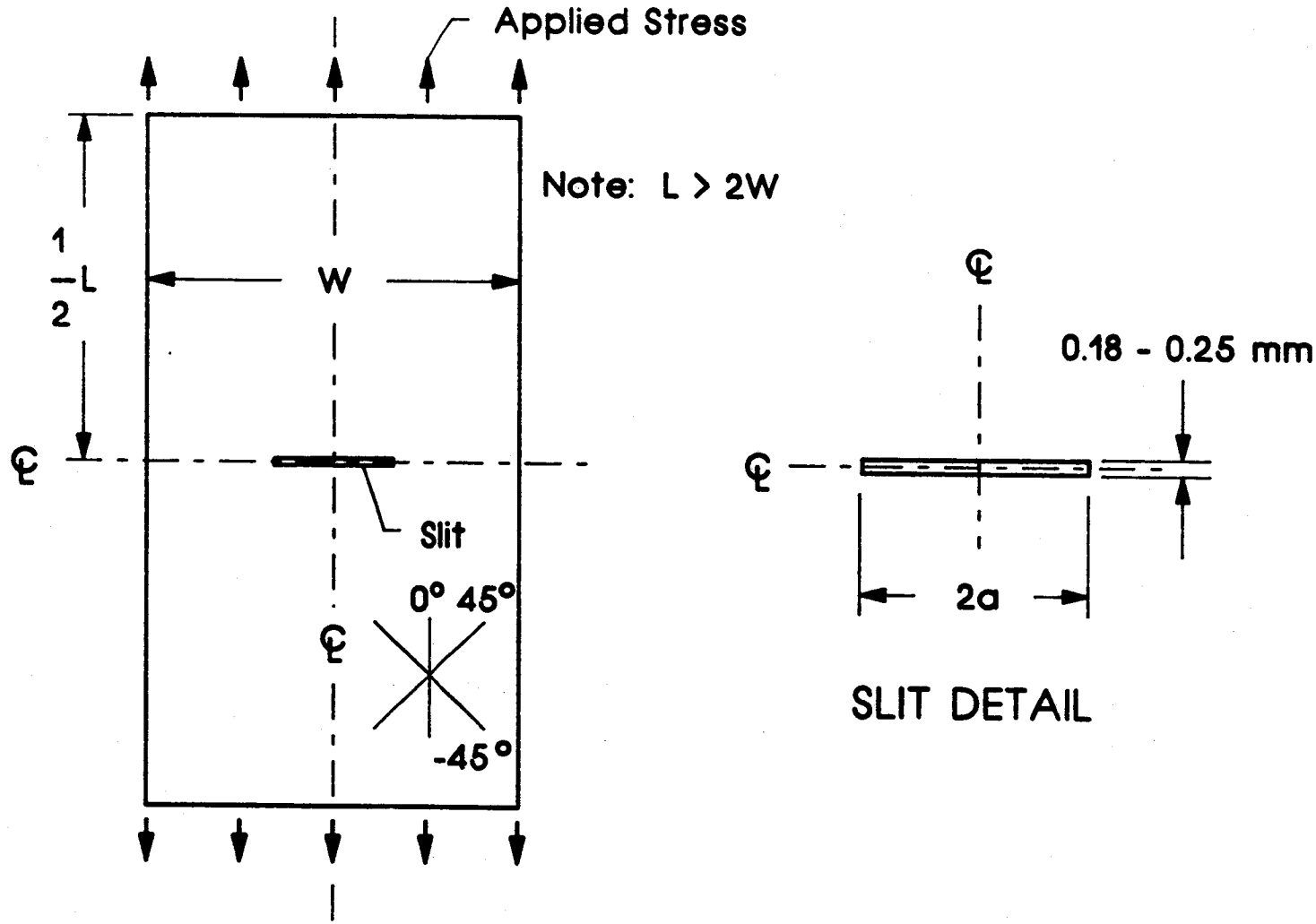

Figure 1.- Sketch of tensile specimen with central crack-like slit.

FIG1.BAL

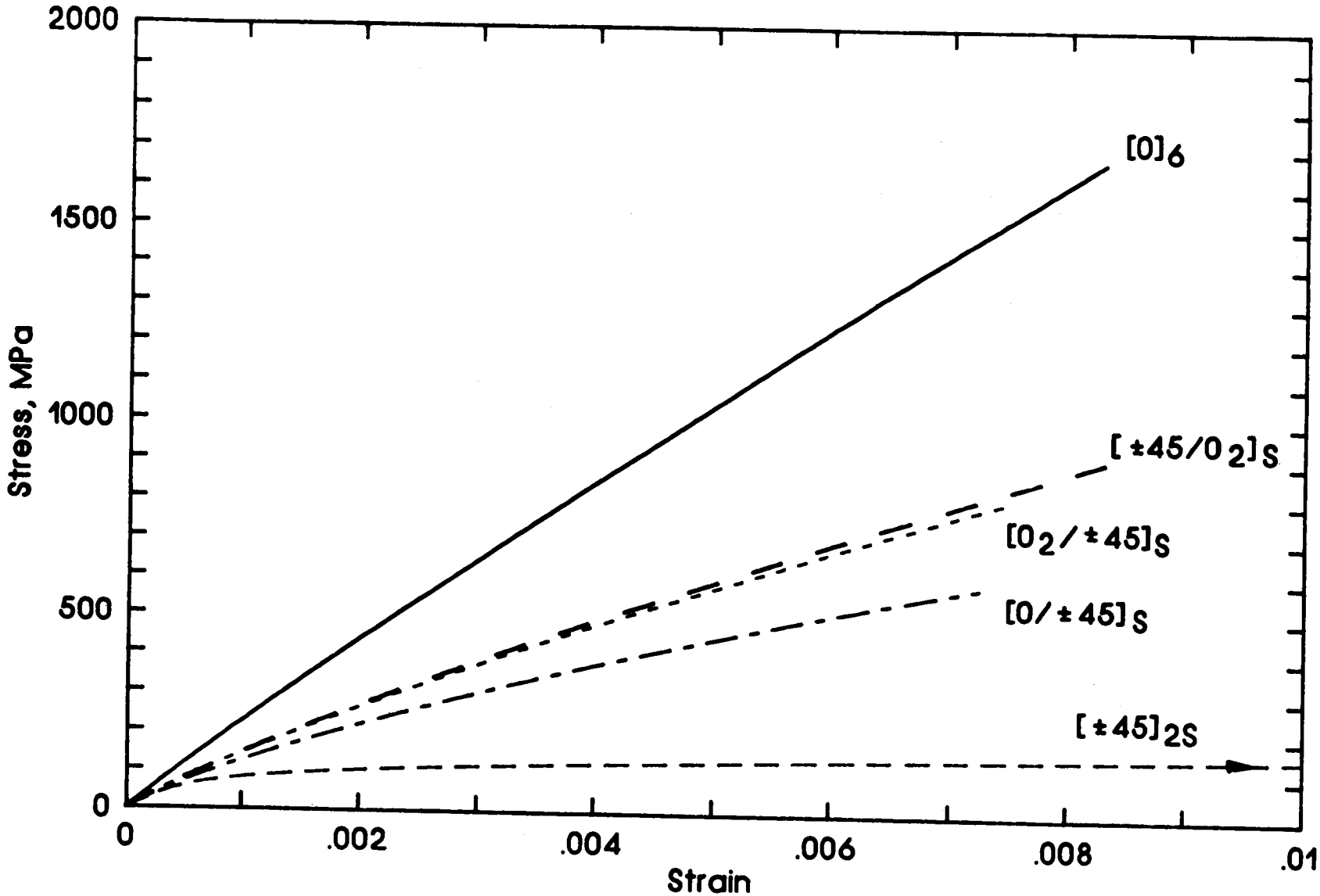

Figure 2.- Calculated stress-strain curves for the various laminate orientations.

FIG2.BAL

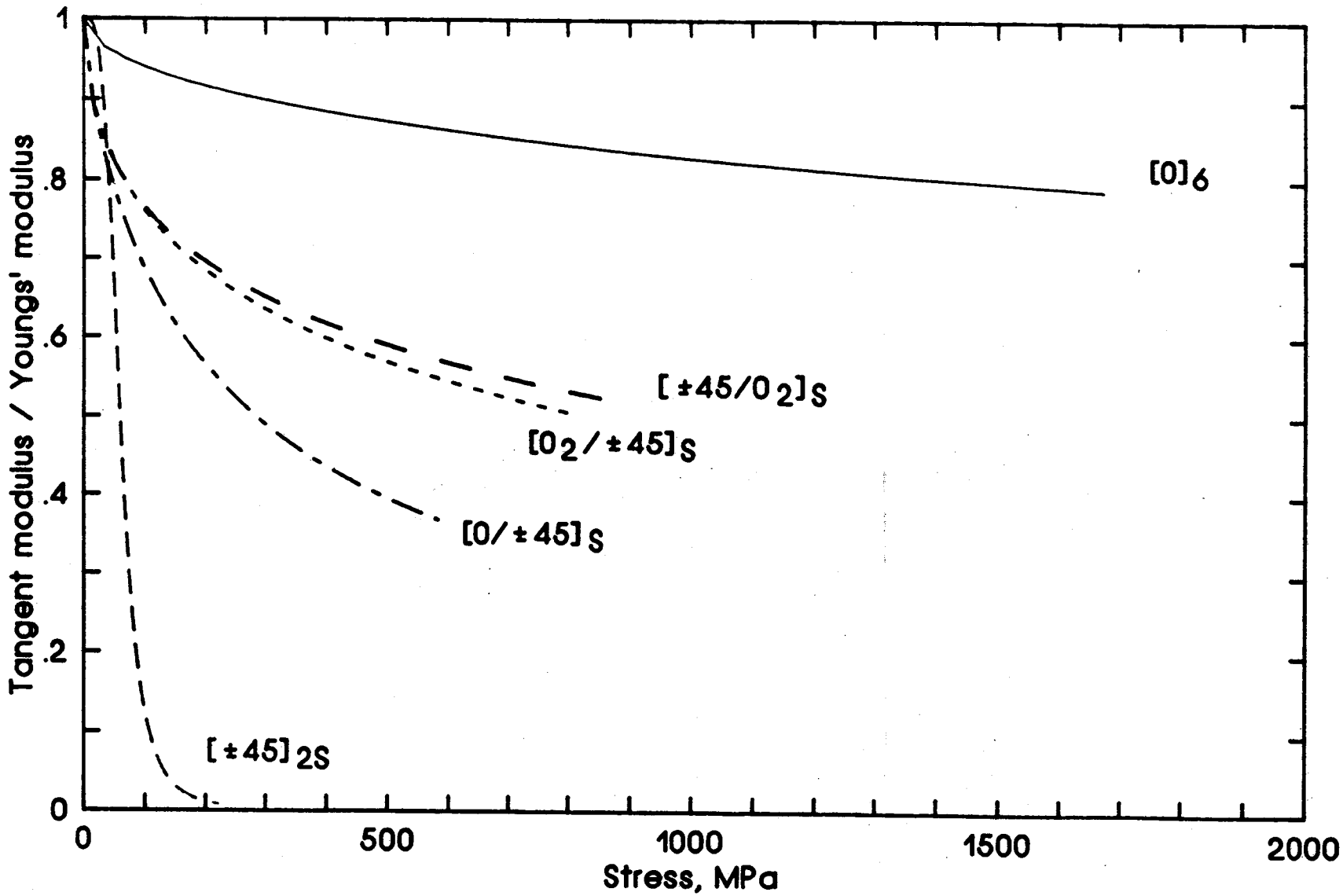

Figure 3.- Calculated tangent modulus versus stress for the various laminate orientations.

FIG3.BAL

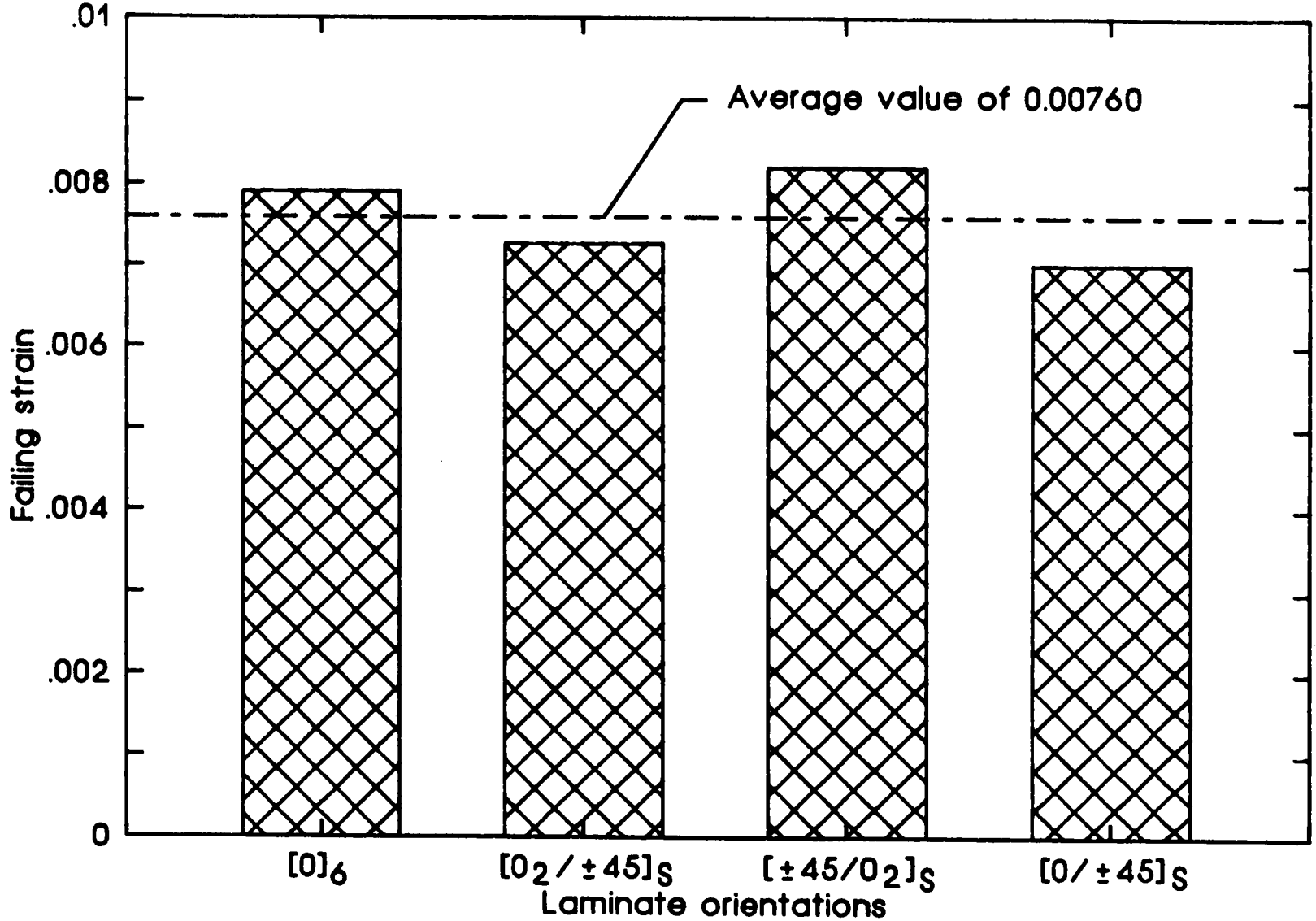

Figure 4.- Failing strains for unnotched specimens with various laminate orientations.

\BAL88\FIG4.BAL

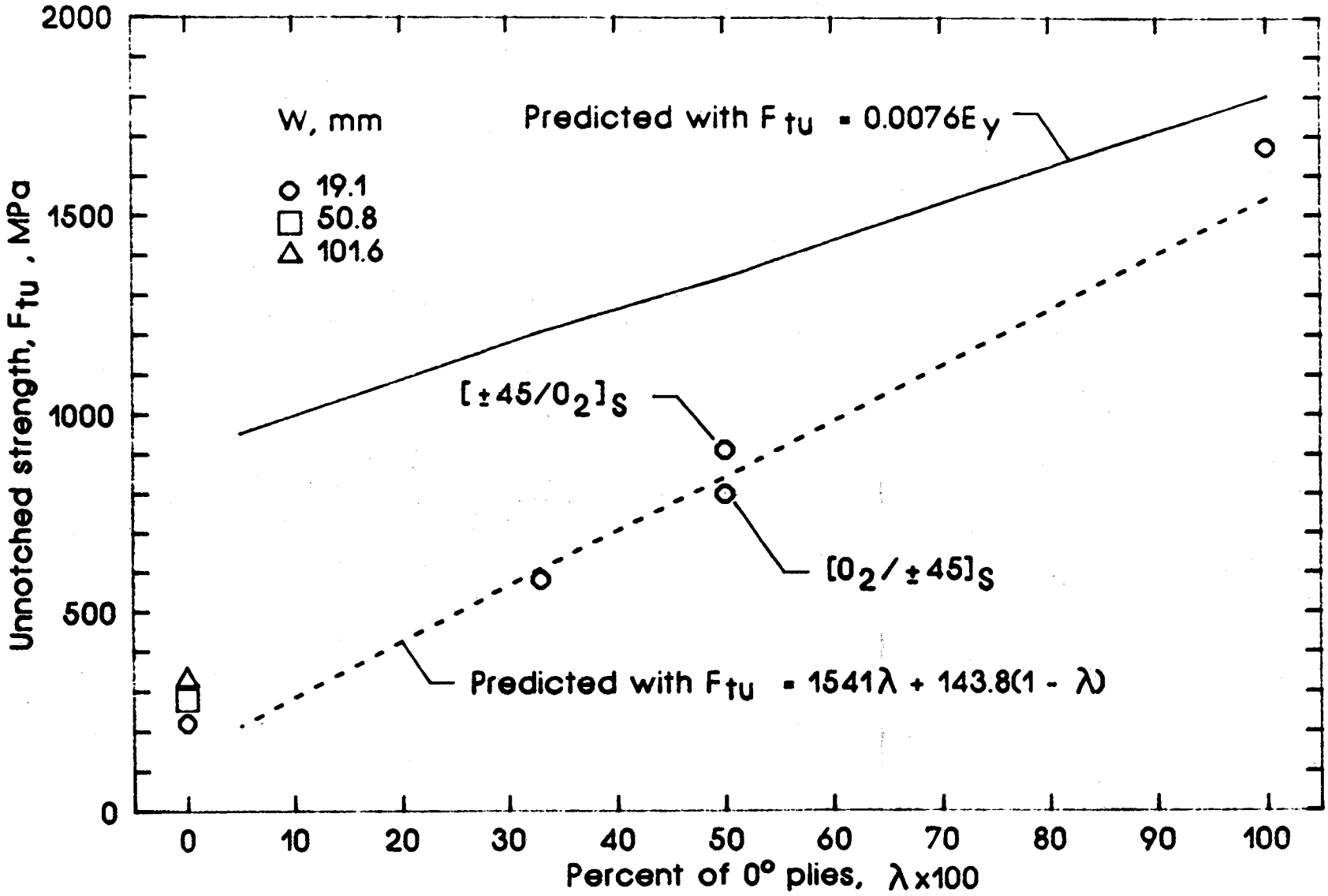

Figure 5.- Unnotched strengths for the various laminate orientations.

\BAL88\FIG5.BAL

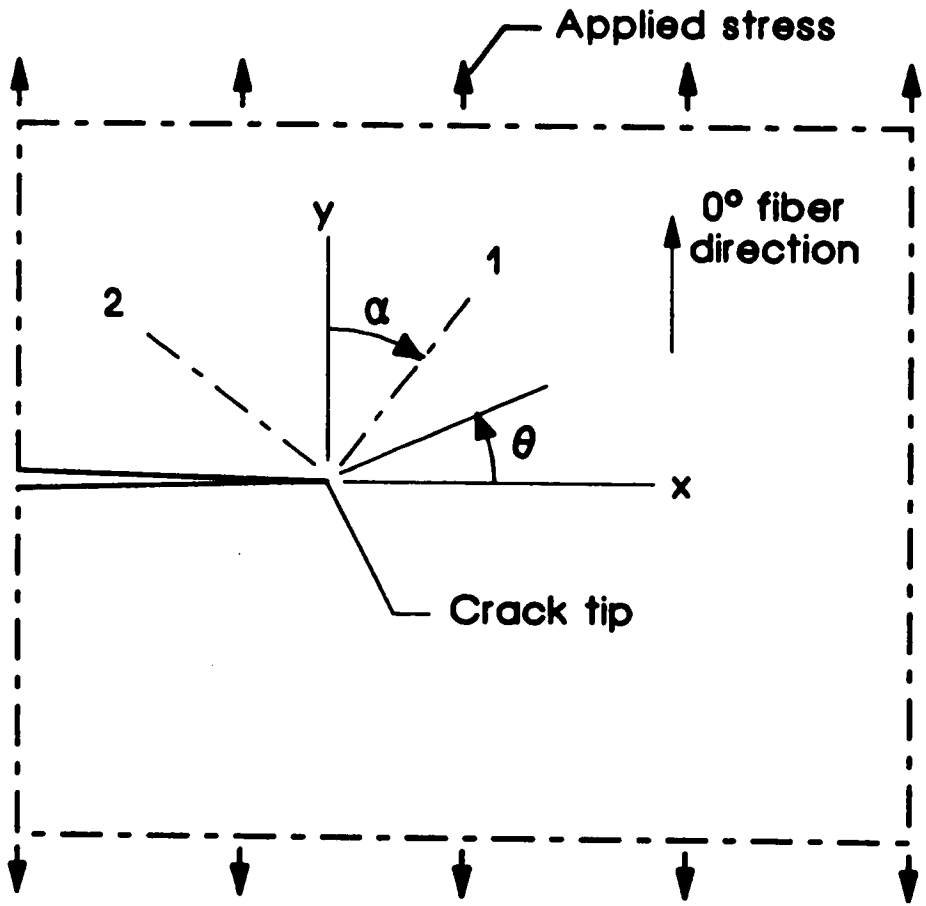

Figure 6.- Laminate and principal lamina coordinates.

FIG6.BAL

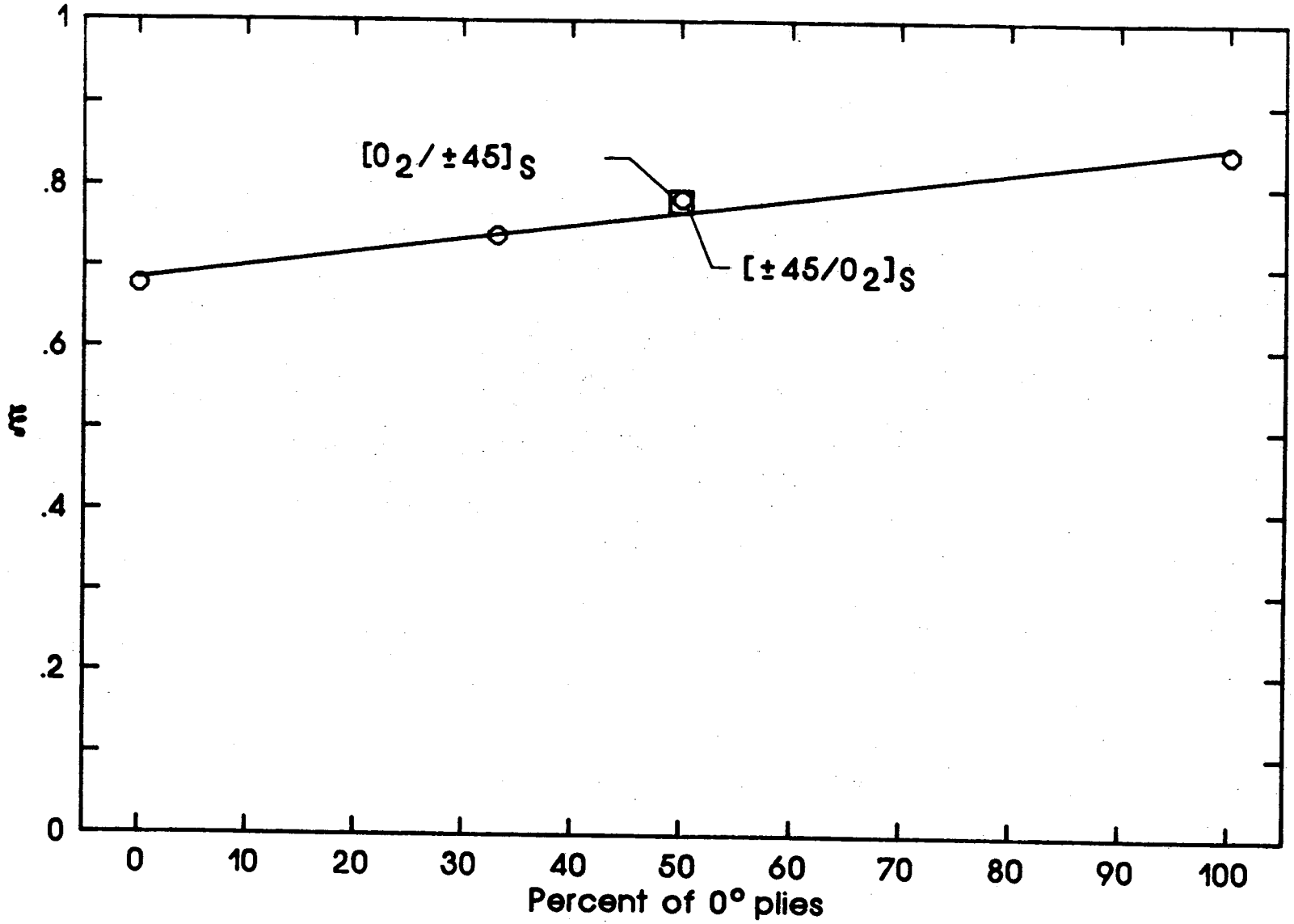

Figure 7.- Nondimensional parameter ξ versus proportion of 0°plies.

\BAL88\FIG7.BAL

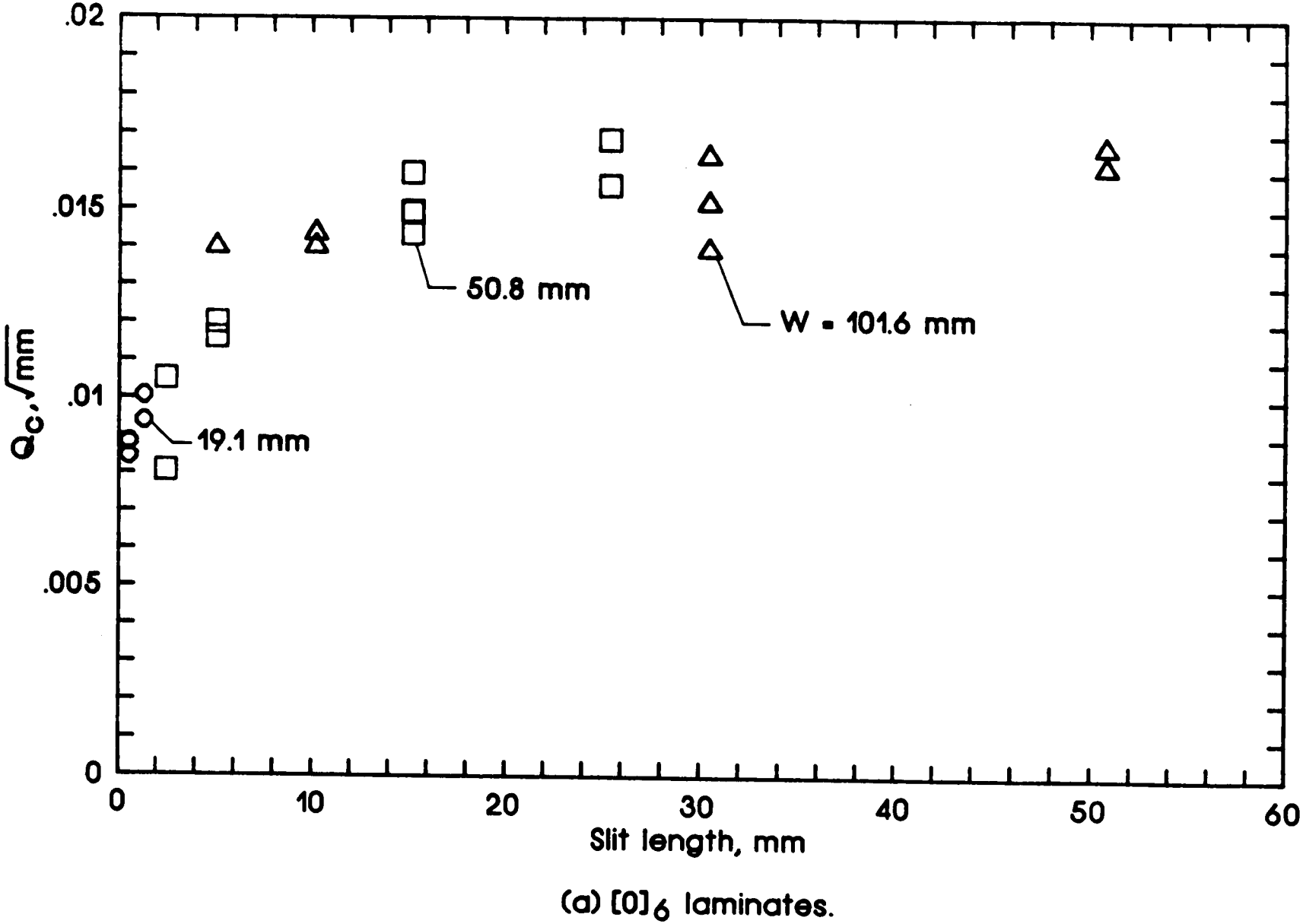

Figure 8.- General fracture toughness parameter versus slit length.

\BAL88\FIG8A.BAL

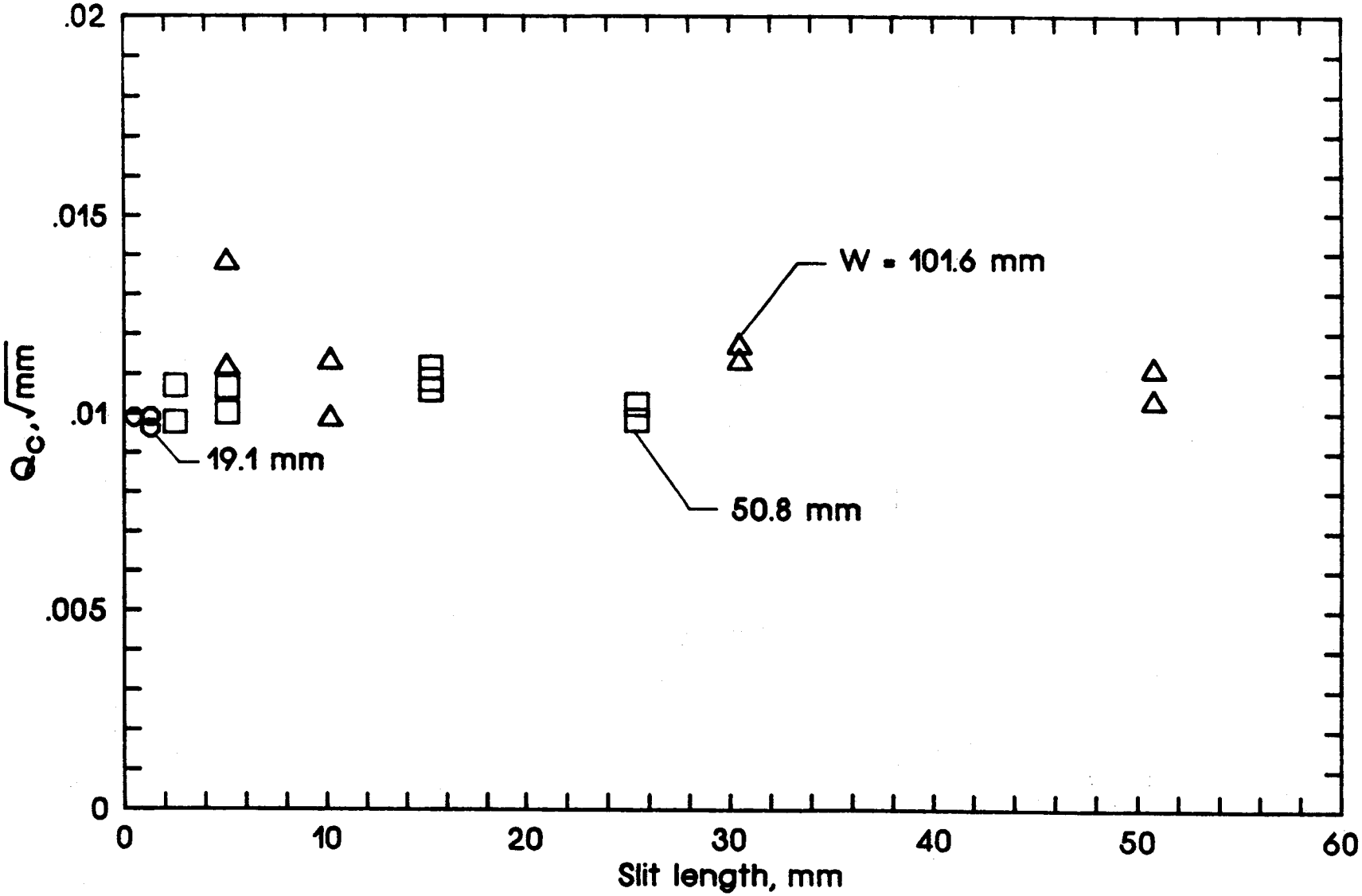

(b) $[0_2 / \pm 45]_S$ laminates.

Figure 8.- Continued.

\BAL88\FIG8B.BAL

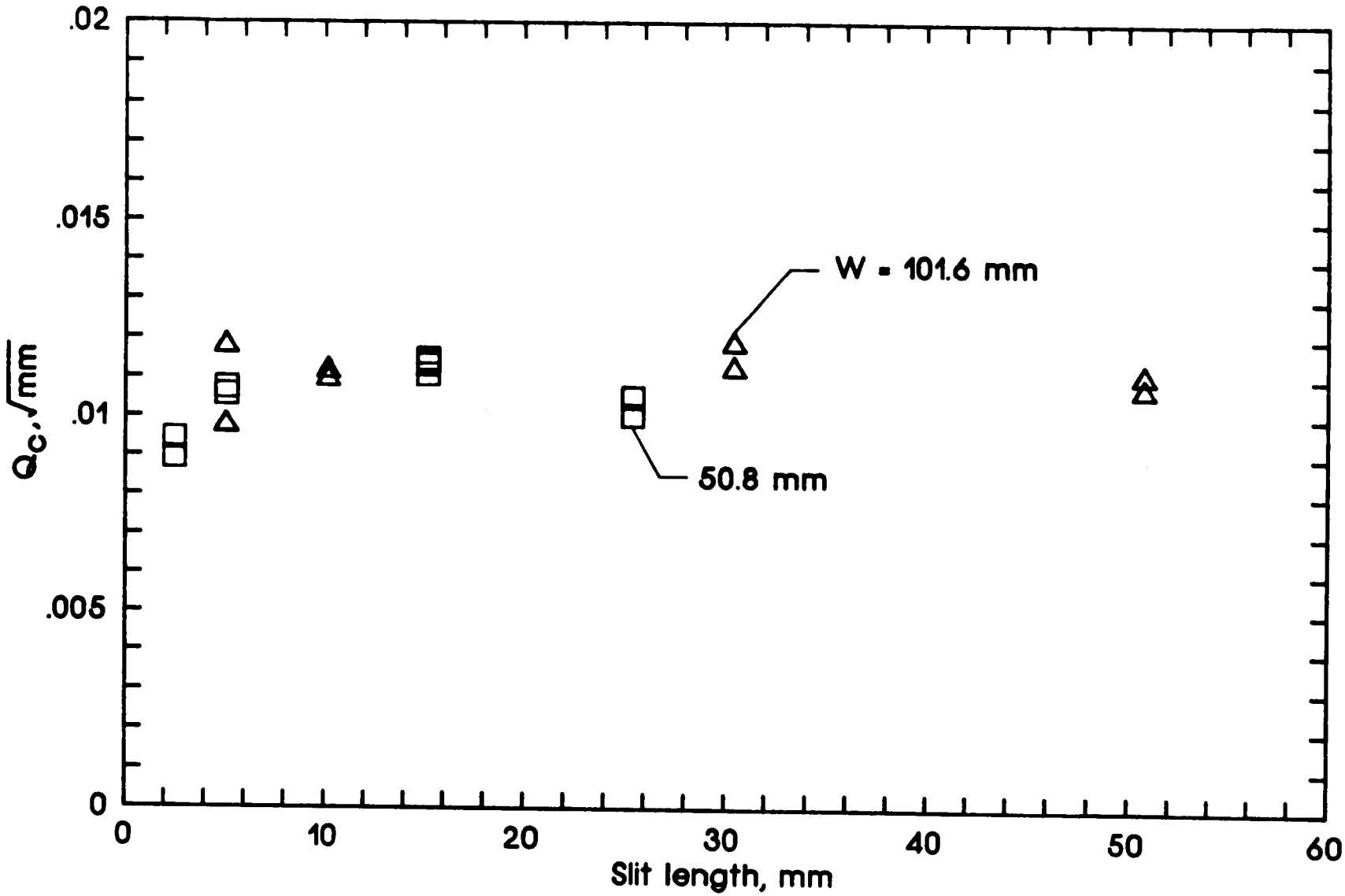

(c) $[\pm 45/0_2]_S$ laminates.

Figure 8.- Continued.

\BAL88\FIG8C.BAL

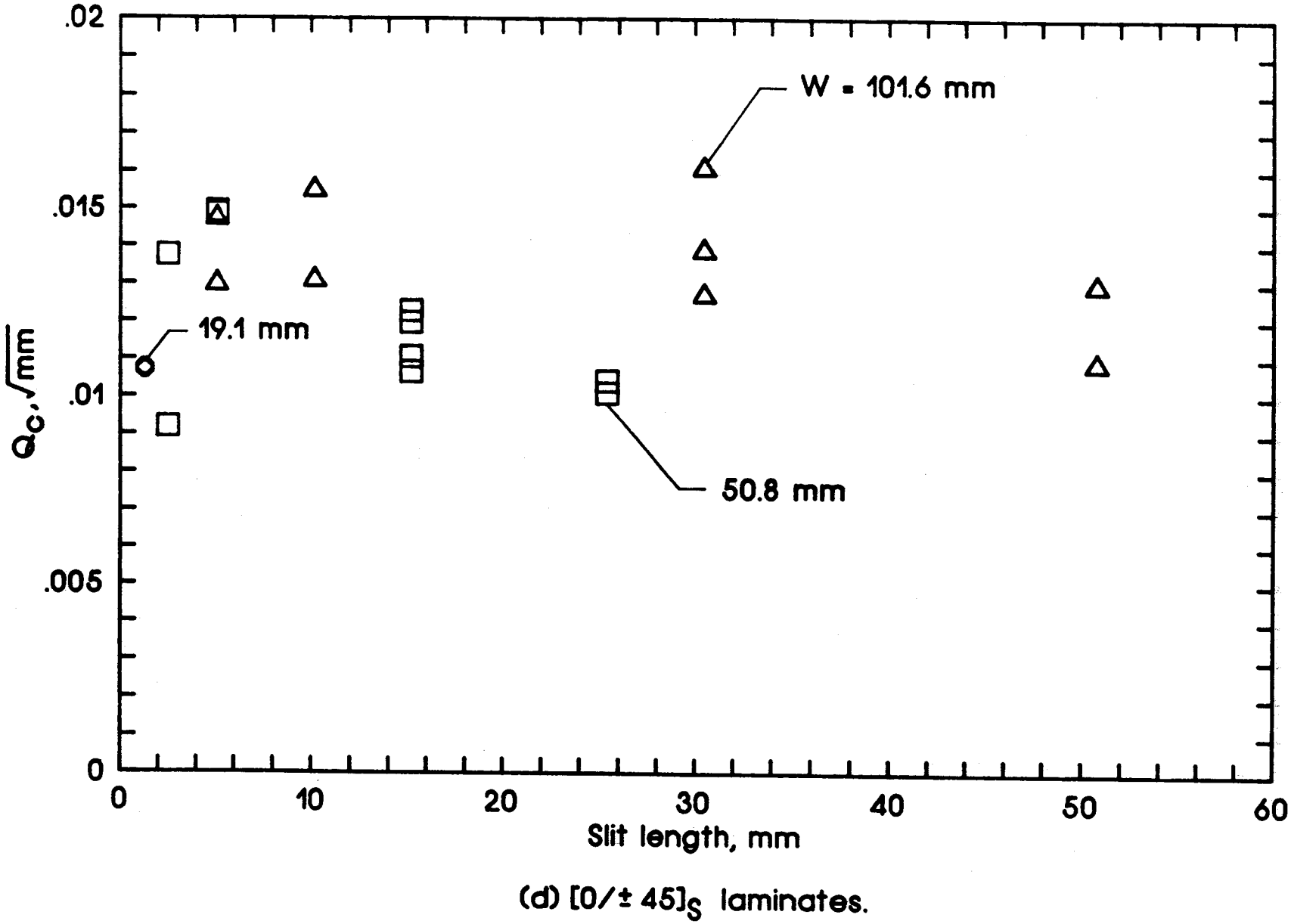

(d) $[0/\pm 45]_S$ laminates.

Figure 8.- Continued.

\BAL88\FIG8D.BAL

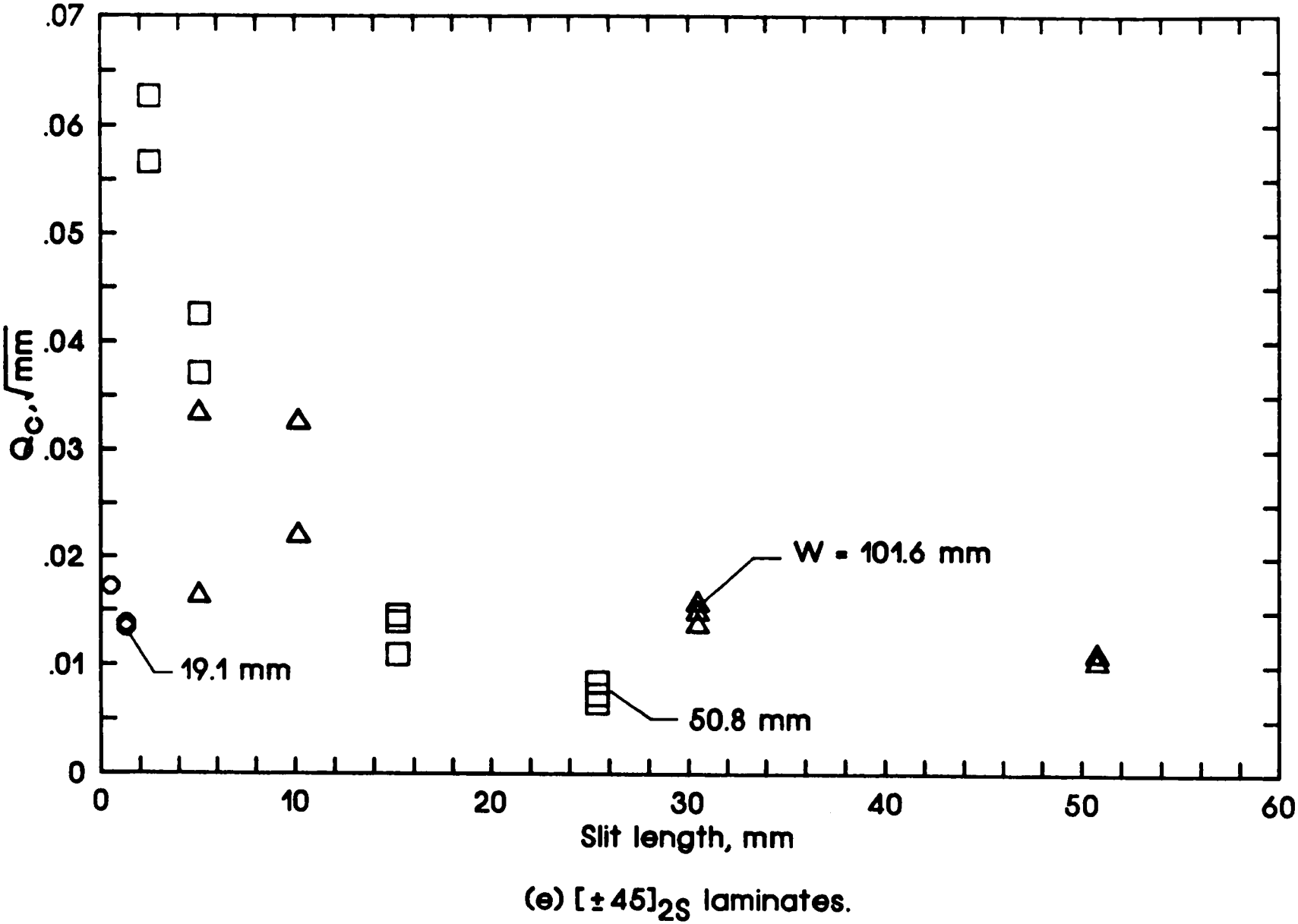

(e) $[\pm 45]_{2S}$ laminates.

Figure 8.- Concluded.

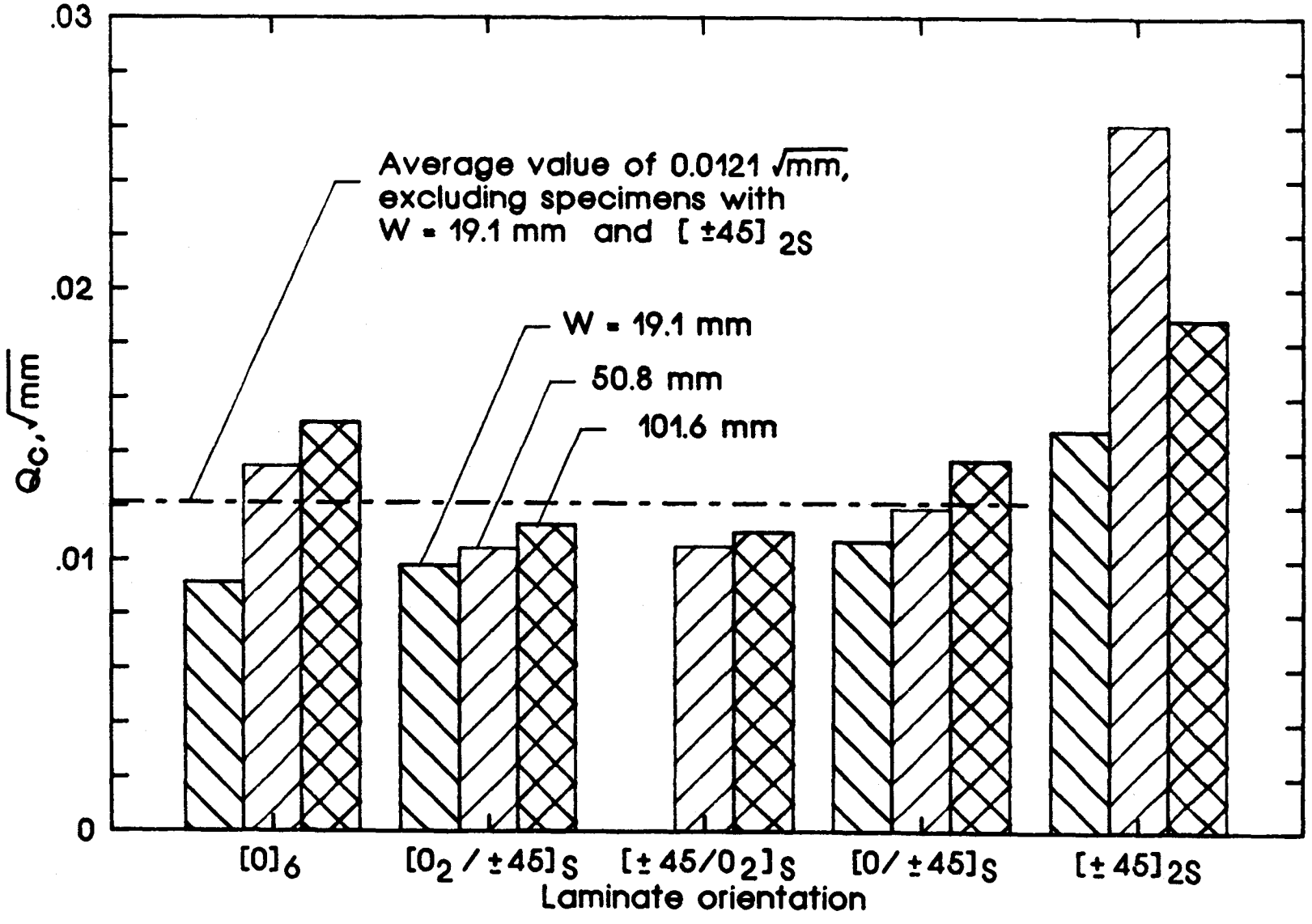

Figure 9.- General fracture toughness parameter for the various specimen widths and laminate orientations.

\BAL88\FIG9.BAL

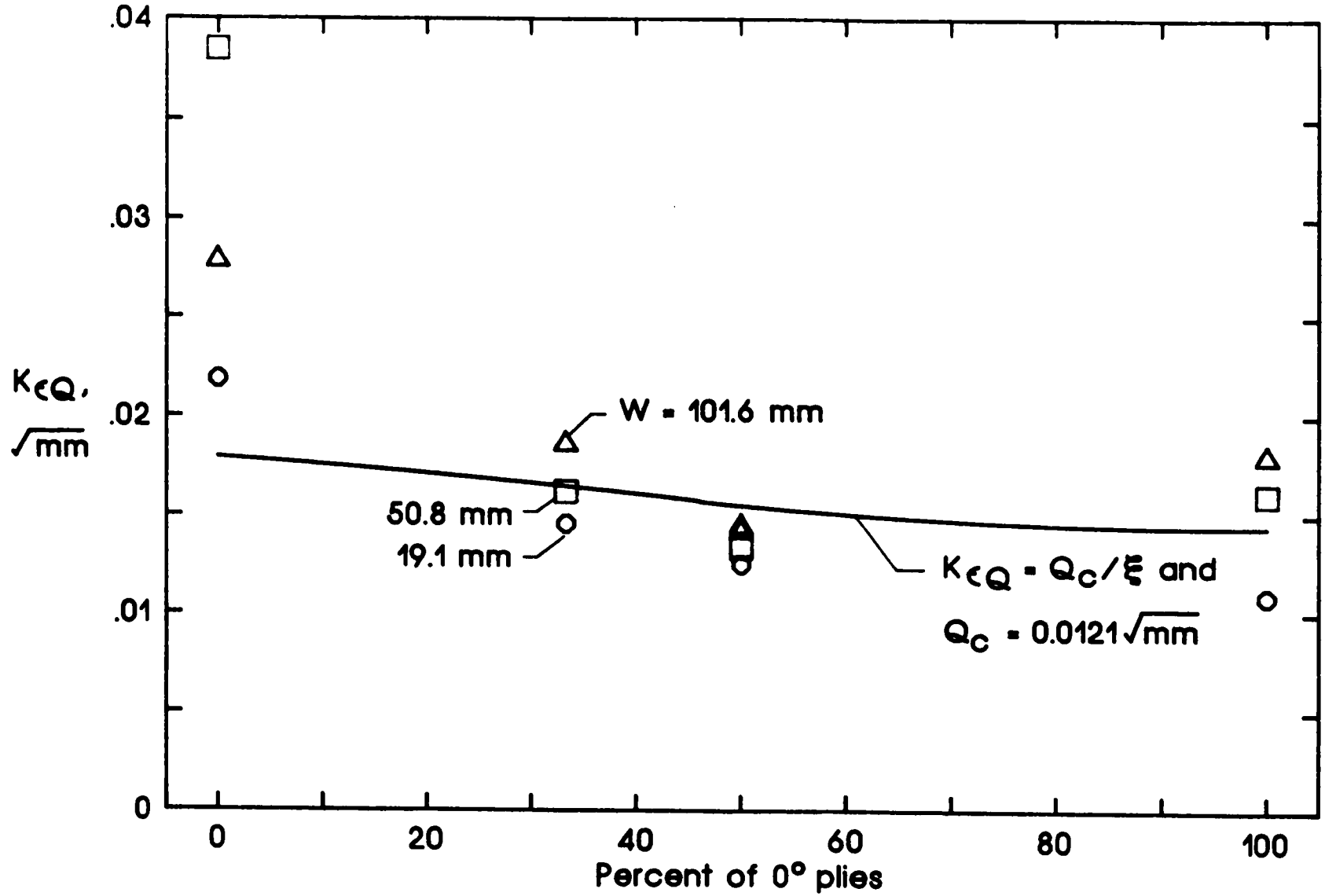

Figure 10.- Predicted and measured values of strain intensity factor at failure.

FIG10.BAL

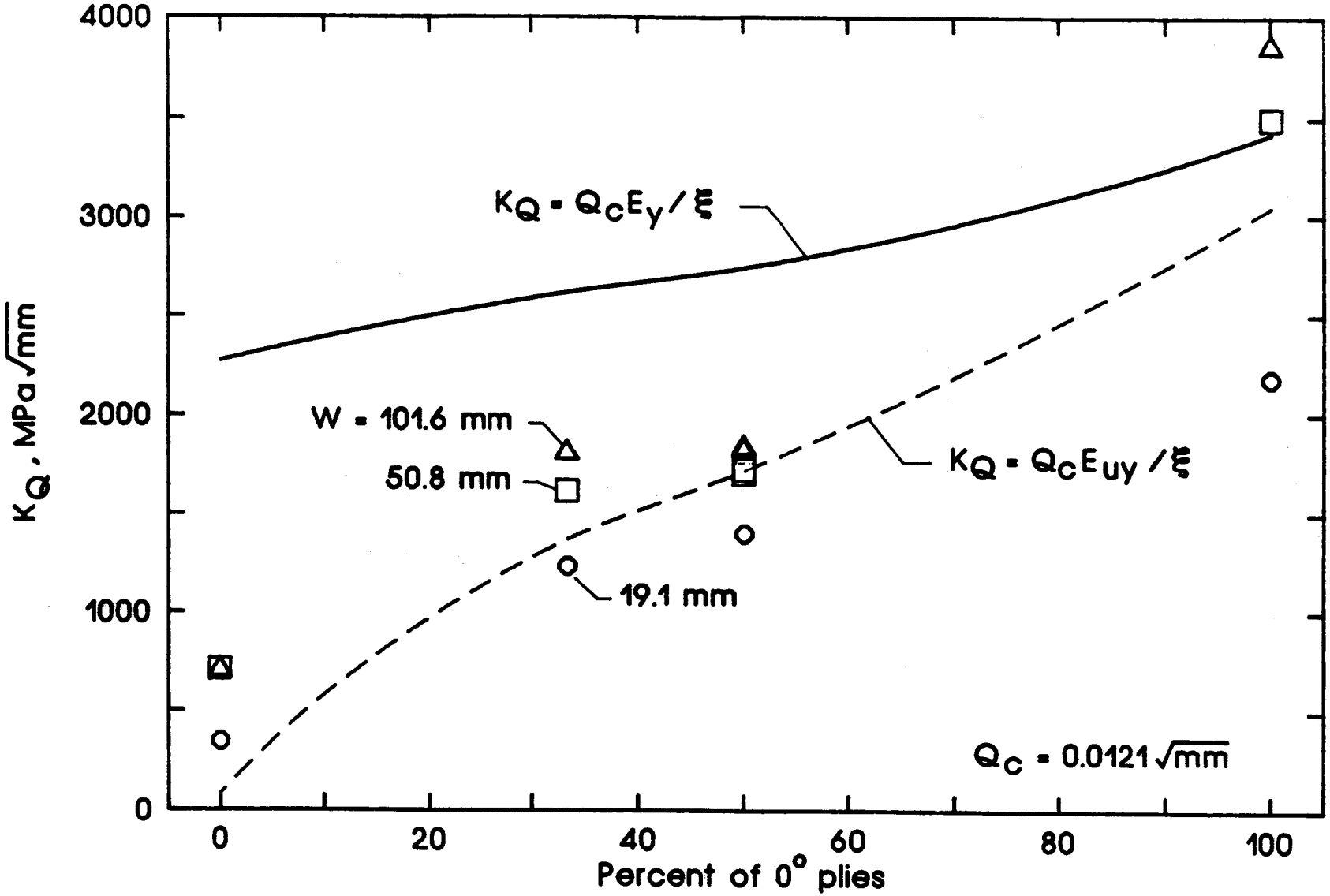

Figure 11.- Predicted and measured values of stress intensity factor at failure.

FIG11.BAL

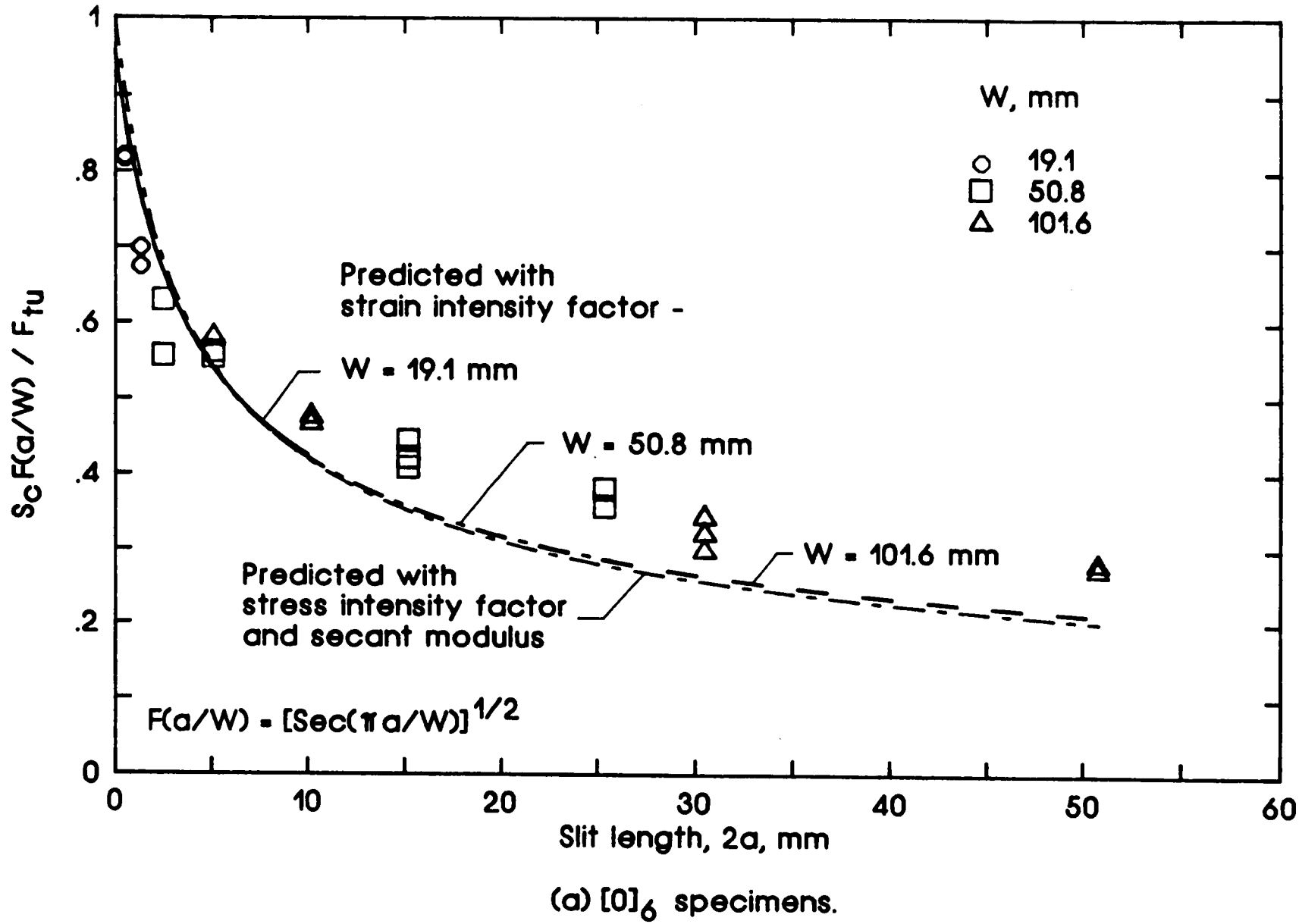

Figure 12.- Measured and predicted strengths for specimens with various laminate orientations.

\BAL88\FIG12A.BAL

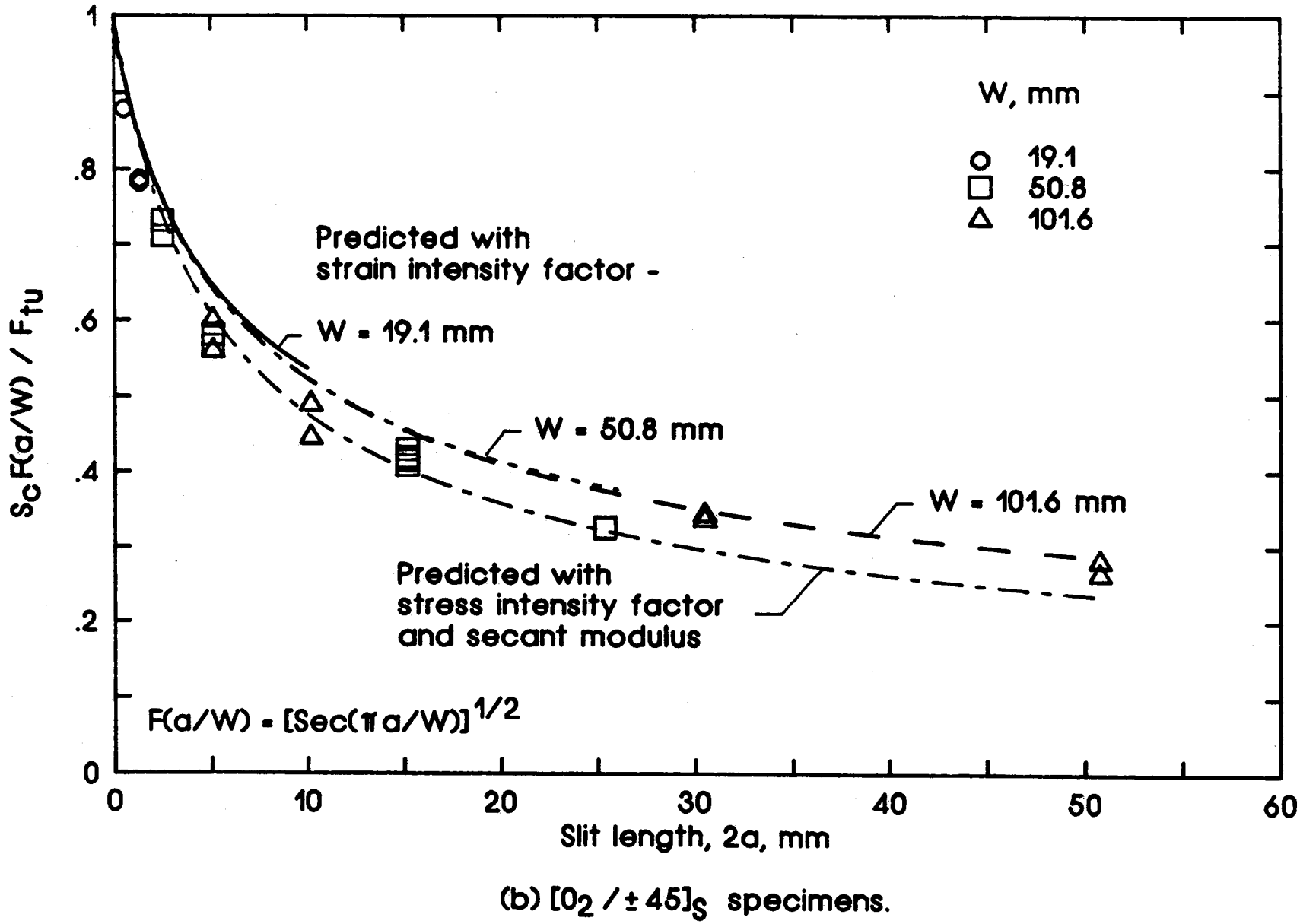

(b) $[0_2 / \pm 45]_S$ specimens.

Figure 12.- Continued.

\BAL88\FIG12B.BAL

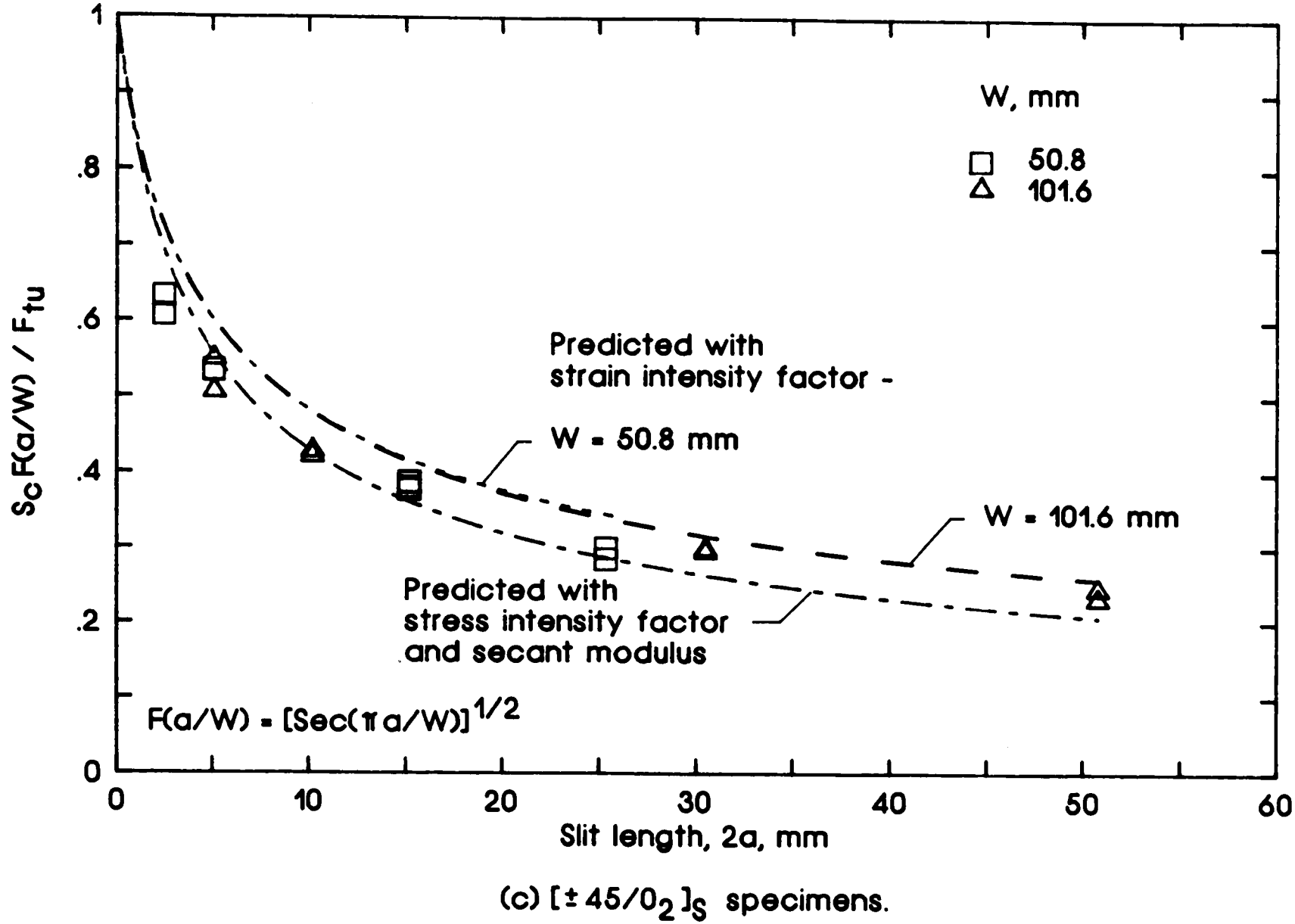

(c) $[\pm 45/0_2]_S$ specimens.

Figure 12.- Continued.

\BAL88\FIG12C.BAL

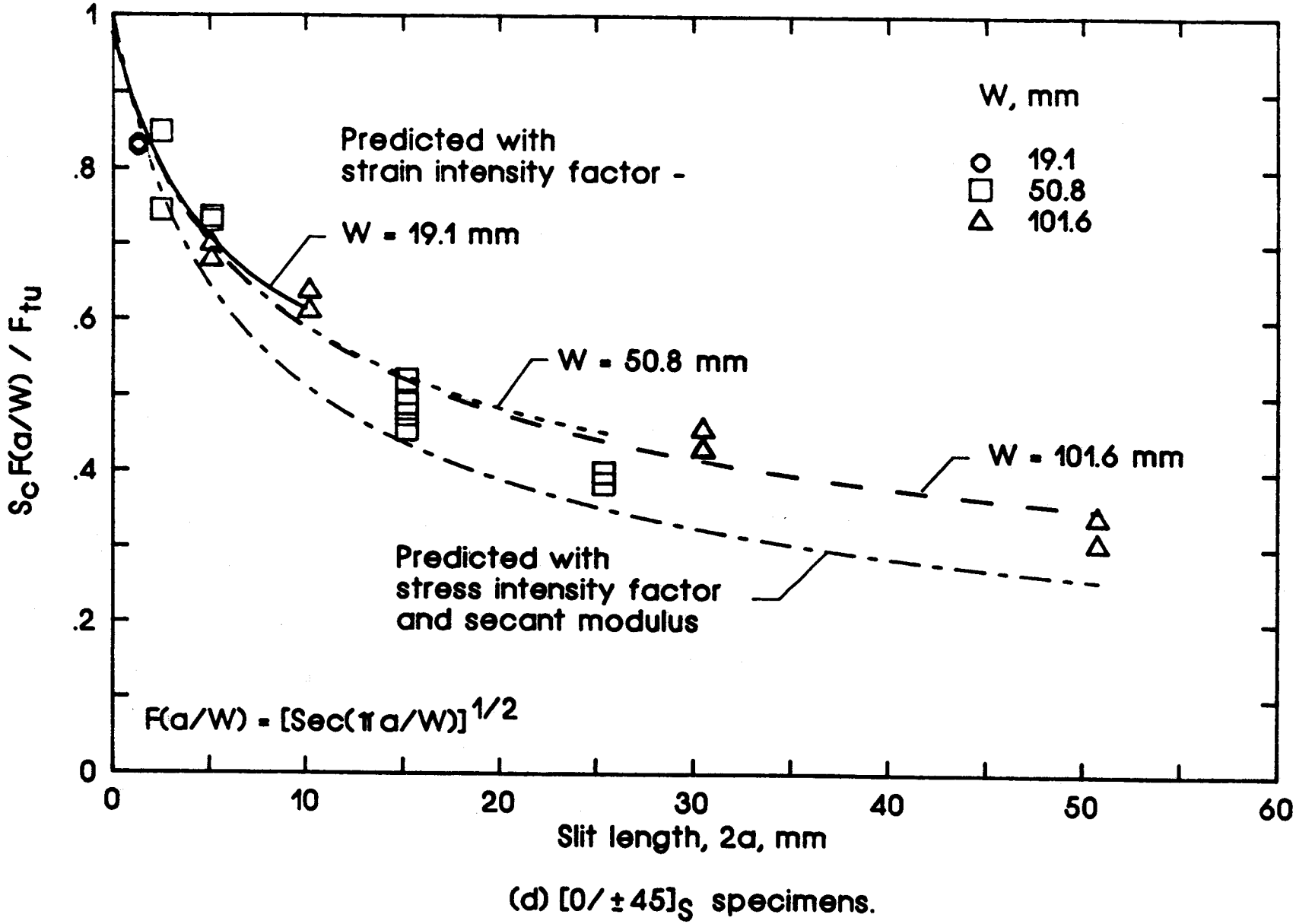

(d) $[0/\pm 45]_S$ specimens.

Figure 12.- Continued.

\BAL88\FIG12D.BAL

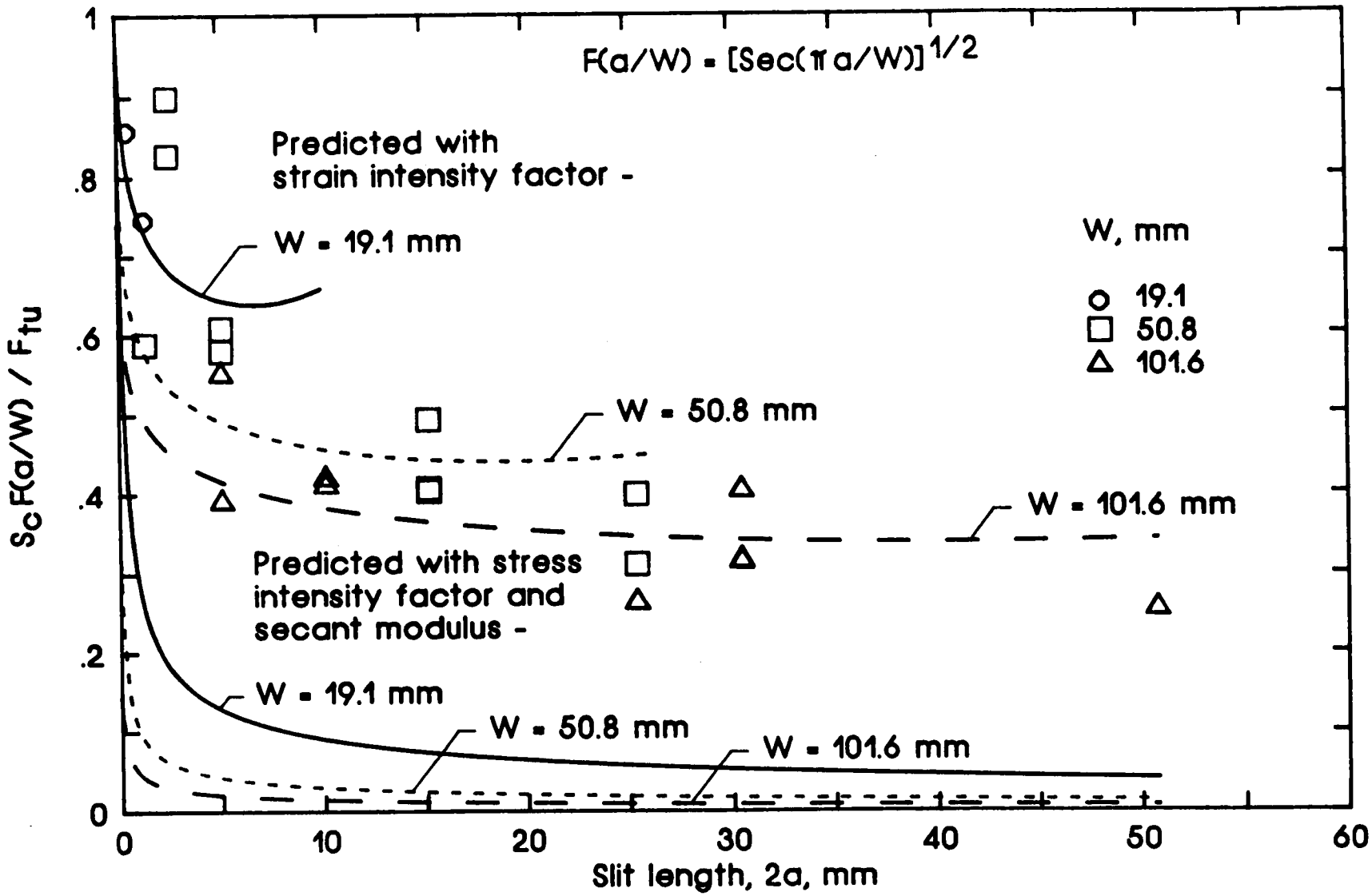

(e) $[\pm 45]_{2S}$ specimens.

Figure 12.- Concluded.

\BAL88\FIG12E.BAL

Standard Bibliographic Page

1. Report No.	2. Government Accession No.	3. Recipient's Catalog No.
NASA TM-100617		

4. Title and Subtitle

STRAIN INTENSITY FACTOR APPROACH FOR PREDICTING THE STRENGTH OF CONTINUOUSLY REINFORCED METAL MATRIX COMPOSITES

5. Report Date: May 1988

6. Performing Organization Code:

7. Author(s)

C. C. Poe, Jr.

8. Performing Organization Report No.:

9. Performing Organization Name and Address

National Aeronautics and Space Administration
Langley Research Center
Hampton, VA 23665-5225

10. Work Unit No.: 506-43-11-04

11. Contract or Grant No.:

12. Sponsoring Agency Name and Address

National Aeronautics and Space Administration
Washington, DC 20546

13. Type of Report and Period Covered: Technical Memorandum

14. Sponsoring Agency Code:

15. Supplementary Notes

16. Abstract

A method was previously developed to predict the fracture toughness (stress intensity factor at failure) of composites in terms of the elastic constants and the tensile failing strain of the fibers. The method was applied to boron/aluminum composites made with various proportions of 0° and ±45° plies. Predicted values of fracture toughness were in gross error because widespread yielding of the aluminum matrix made the compliance very nonlinear. An alternate method was developed to predict the strain intensity factor at failure rather than the stress intensity factor because the singular strain field was not affected by yielding as much as the stress field. Strengths of specimens containing crack-like slits were calculated from predicted failing strains using uniaxial stress-strain curves. The predicted strengths were in good agreement with experimental values, even for the very nonlinear laminates that contained only ±45° plies. This approach should be valid for other metal matrix composites that have continuous fibers.

17. Key Words (Suggested by Authors(s))	18. Distribution Statement
Composite materials Metal matrix Fracture mechanics Stress intensity factor Strain intensity factor Boron/aluminum Strength Fracture toughness	Unclassified - Unlimited Subject Category - 24

19. Security Classif.(of this report)	20. Security Classif.(of this page)	21. No. of Pages	22. Price
Unclassified	Unclassified	36	A03

For sale by the National Technical Information Service, Springfield, Virginia 22161